Studies on Optimisation of Processing Parameters for Ultra-thin CdTe Solar Cell

Chandan Bhardwaj

Submitted for the degree of Master of Philosophy

Heriot-Watt University

School of Engineering and Physical Sciences

September 2015

ABSTRACT

Ultra-thin solar cell devices can have many potential applications as top cells in tandem solar cells as well as power generating window material in buildings. Such applications require that ultra-thin layers should be easy to fabricate, have very high optical transparency to allow maximum light to pass through, generate high power and be low cost.

CdTe based ultra-thin cells are suitable candidates for such applications. Less than 1 micron thick layers of CdTe can be high on transmittance and yet absorb good percentage of incident photons. Optical and electrical properties ultra-thin devices based on CdTe need to be investigated to examine its suitability for use in tandem cells or building materials.

This research is focused on fabricating solar cells with increasingly thinner CdTe layer (< 1 μm) on glass based and flexible substrates. Low cost methods such as electrodeposition and chemical bath deposition were used to deposit solar cell layers. Computer Modeling was carried out to design and optimize the optical transparency and output power of the solar cells produced. Ultra-thin solar cells prepared by MOCVD had efficiency of 4.9 % for a 400 nm thin CdTe layer cell. Experimental results showed very good agreement with the modeling results. Use of $Cd_{1-x}Zn_xTe$ has an absorber material has also been investigated using modeling.

ACKNOWLEDGEMENTS

I would like to sincerely thank Prof. Hari M Upadhyaya for his supervision and guidance. I would also like to thank Dr. Senthilarasu Sundaram for his continuous support and guidance.

The useful inputs by my colleagues Dr. Prabhakar Bobilli and Zhengfei Wei are sincerely appreciated.

I would also like to extend my special thanks to Dr. Andy Clayton for depositing MOCVD based ultra-thin CdTe films.

ACADEMIC REGISTRY
Research Thesis Submission

Name	Chandan Bhardwaj		
School/PGI:	Engineering and Physical Sciences		
Version: *(i.e. First, Resubmission , Final)*	Final	Degree Sought (Award **and** Subject area)	M Phil Mechanical Engineering

---

Declaration

In accordance with the appropriate regulations I hereby submit my thesis and I declare that:

1) the thesis embodies the results of my own work and has been composed by myself
2) where appropriate, I have made acknowledgement of the work of others and have made reference to work carried out in collaboration with other persons
3) the thesis is the correct version of the thesis for submission and is the same version as any electronic versions submitted*.
4) my thesis for the award referred to, deposited in the Heriot-Watt University Library, should be made available for loan or photocopying and be available via the Institutional Repository, subject to such conditions as the Librarian may require
5) I understand that as a student of the University I am required to abide by the Regulations of the University and to conform to its discipline.

* *Please note that it is the responsibility of the candidate to ensure that the correct version of the thesis is submitted.*

Signature of Candidate*:*	CBhardwaj	Date:	3/9/2015

Submission

Submitted By *(name in capitals):*	CHANDAN BHARDWAJ
Signature of Individual Submitting:	CBhardwaj
Date Submitted:	3/9/2015

For Completion in the Student Service Centre (SSC)

Received in the SSC by *(name in capitals):*			
Method of Submission (Handed in to SSC; posted through internal/external mail):			
E-thesis Submitted ***(mandatory for final theses)***			
Signature:		Date:	

TABLE OF CONTENTS

Chapter 1: Introduction

The energy demand in the world is increasing at a rapid rate [1]. As the countries become more and more industrialized, per capita consumption of electricity increases. While on one hand growth brings prosperity to a nation it also puts immense pressure on the earth's resources. Fossil fuels – coal, petroleum have been the main energy source for the last two centuries. However, these reserves are fast depleting. Moreover their increased usage generates vast amounts of greenhouse gases that put the nature at risk. Alternative forms of energy are an urgent need of the hour.

Solar energy can be a major source of energy for this planet's needs. It is available in abundance and is environment friendly. The photovoltaic (PV) technology now a major industry exists, which can directly convert solar energy into electricity [2]. The advantage of the PV technology is that it is modular in nature that is a system size can range from few kWs to few MWs simply by placing modules in series and parallel. Also photovoltaic modules are passive no noise and no pollution emitting systems that can be placed anywhere from deserts to rooftops. It is estimated that 0.3 per cent of land covered by solar modules are enough to take care of almost all of earth's electricity needs. In the wake of depleting fossil fuel reserves, photovoltaic cells have a very important role to play. A commonly used standard is the AM 1.5, according to which solar intensity incident is taken at $1000W/m^2$. Thus it has a lot of scope in being used as energy provider in remote locations which are difficult to connect with the central electricity grid. Another very important application is that PV cells can be incorporated into a building envelope products such as windows or roof shingles [3].

Solar cells first gained prominence in the 1960's [4] but the focus was only on demonstration of the photovoltaic nature of various semiconductors. By 1980's, [4] emphasis shifted towards manufacturing of solar cells. Solar cells found important use in powering satellites. During this time the majority of solar cells made were based on crystalline silicon (c-Si) as the *p-n* junction. Since then silicon based solar technology, led by c-Si has been the mainstay of the PV industry covering around 90 % of the solar cell production. Crystalline-Si cells have benefited from the scientific and industrial infrastructure available for integrated circuits used in the electronics industry. The basic component is the *p-n* junction in ICs as well as solar cells. Manufacturing units were already in place and high purity silicon was readily available. PV industry could build on the research already carried out the semiconductor industry. In addition silicon is a

very abundant material. Thus raw material availability is not a major issue even for TW scale cell production.

The PV industry mainly depends on the Silicon based solar cells which involves an energy intensive process. The costs of solar cells have prevented the deployment of solar modules on large scale. Electricity from PV is still at least three times higher than other forms of energy. To address the cost issue of solar cell, newer semiconductors have been researched as an alternative technology for solar cells. Thin film solar cells thus gained prominence which is different from crystalline silicon because the absorbers in thin film solar cells are much thinner [5]. These thin film layers can be deposited on a variety of substrates and can be deposited at low temperatures [6]. Effectively thin film solar cell technologies allow cells to be produced at much lower costs and using much simpler methods. Of the various thin film technologies, amorphous silicon (a-Si), copper indium gallium selenide (CIGS) and cadmium telluride (CdTe) have proved better in terms of efficiency, stability and manufacturability [7].

Amorphous silicon is mainly prepared by a method called plasma enhanced chemical vapour deposition [8]. In this method, gases like SiH_4 (silane) are used to deposit a-Si under plasma conditions. The process is a low temperature process as the temperatures are kept between 150 – 350 ^oC. This method allows a variety of substrates to be used such as glass, stainless steel or even fabric. Amorphous silicon solar cell efficiency is around 8-9 %. These cells are typically multi-junction cells. However, they suffer from stability issues because their efficiency degrades upon continuous illumination through a phenomenon referred to as Staebler–Wronski Effect (WRE), as the cells gradually stabilize.

$Cu(InGa)Se_2$ or CIGS is another promising solar technology. CIGS absorber is commonly deposited by two methods. In one method, the constituent elements of copper, indium, gallium and selenium are evaporated together and allowed to deposit simultaneously to form layers on a substrate heated to around 500-600^o C in a single step. In the other method, deposition of CIGS components is done sequentially. First copper, indium and gallium layers are deposited on a substrate using methods such as electrodeposition or sputtering. Then the substrate is heated in selenium ambient, typically with nitrogen as carrier gas [7]. CIGS cells have reported the maximum efficiency over 20%. The scarce availability of indium is a major issue in large scale production of CIGS cells.

Thin film solar cells based on CdTe are very popular because they can be prepared by variety of simple methods. CdTe films are also very stable. Some more popular methods for preparing CdTe thin films are electrodeposition (ED), close space sublimation, sputtering, metal organic chemical vapour deposition and spray pyrolysis. CdTe solar cells have had highest efficiency of 17.3 % [9].

The thin film solar cell technology holds great promise as it can bring down the cost of energy from PV considerably. One very promising field of application for thin film solar cells is Building Integrated Photovoltaics (BIPV). This means that the solar cell material is built into the windows or other building materials. When integrated into windows, this PV window element can be architecturally unobtrusive as well as generate power. An output power of ~ 50W/m^2 has been reported when incident sunlight of 600 W/m^2 falls on semi-transparent skylight made of mutli-crystalline silicon [10]. Visible transmittance for the system studied in [10] was about 20 %. Visible transmittance values for typical double pane windows are ~ 76 % [11]. Suitable designing can reduce or increase solar gains depending upon the nature of outside environment. Such applications require that the solar cell device have high enough optical transparency. The layers of the device need to be ultra-thin for this purpose. This also requires that the fabrication procedure should have very good control over the thickness of layers. The challenge is then to demonstrate such a device prepared by low cost methods that increases the utility of a building material without too much additional costs.

CdTe, a II^B-VI^A compound semiconductor has certain properties that make it a suitable candidate as an absorber material in solar cells for photovoltaic energy conversion. It has an energy band gap, E_g = 1.5eV [12] which closely matches the solar spectrum. It also has a high absorption coefficient > 10^5/cm [12] which allows even a thin layer of CdTe to absorb photons over a large wavelength range from the solar spectrum. Thus material utilization will be very efficient thus keeping costs to a minimum. CdTe proposes to be a good candidate for BIPV applications.

Trying to produce good quality thin film CdTe thickness requires good process control. Of the various methods for depositing CdTe, sputtering, metal organic chemical vapour deposition and electrodeposition are methods that allow very good process control. Electrodeposition is a low cost method. It allows low temperature (~200^{o}C) sequential deposition of CdS and CdTe layer on transparent conducting oxide (TCO) coated glass

substrates and other substrates such as Aluminum, steel etc. It allows good control over the thickness of the thin film, typical deposition rates being ~0.05 μm/ min.

Cadmium zinc telluride is semiconductor material, which is a solid solution between CdTe and ZnTe semiconductors. Its band gap can be varied between 1.45 -2.25eV [13, 14]. This absorber layer can be deposited using similar methods as CdTe. A higher band gap gives the scope for higher transmittance for $Cd_{1-x}Zn_xTe$ compounds.

Thus this work focused on the following issues

a) Fabrication and characterization of ultra-thin CdTe films using electrodeposition.
b) Theoretical simulation of CdTe solar cell stack by selecting different thickness of CdTe layer with two different thick CdS window layers and its optical transparency and device characterization.
c) Comparison of theoretical modeling with experimentally prepared CdTe solar cells.
d) Moreover, to replace the CdTe absorber layer, theoretical simulation of optical transparency on CZT ($Cd_{1-x}Zn_xTe$) group of compounds as absorber in ultra-thin film solar cells have also been performed and added in the thesis.

Chapter 2 discusses the theoretical aspects of solar cells. It explains the basics of a solar cell and discusses properties of CdTe and its deposition methods. Then it describes the structure and various layers of a CdTe based solar cell.

Chapter 3 describes the electrodeposition process. The experimental details of CdTe film deposited on FTO/Glass substrates by electrodeposition are described. Characterization of these deposited layers has been carried out and is reported.

Chapter 4 reports the results and discussion on ultra-thin film solar cells prepared by MOCVD (metal organic vapour deposition) grown CdTe on chemical bath deposited CdS. The study was jointly carried out with Dr. Andrew Clayton at CSER (Centre for Solar Energy Research) at Glyndŵr University.

Chapter 5 describes the optical modelling of a simple CdTe based solar cell stack. The modelling has been carried out using a software called CODE (Coating Designer). The modelling results have been compared with experimental results observed in chapter 4.

Chapter 6 presents optical modelling results for a CZT based solar cell stack. The possibility of using CZT as absorber in place of CdTe has been discussed.

Chapter 2: Thin Film Solar Cells

2.1 Introduction

A solar photovoltaic cell is a device that converts light energy from the sun into electrical energy. This is achieved by a semiconductor *p-n* junction, which on action of light results in the charge separation across the junction through the existing built-in electric field in the depletion region as shown below in figure 2.1.

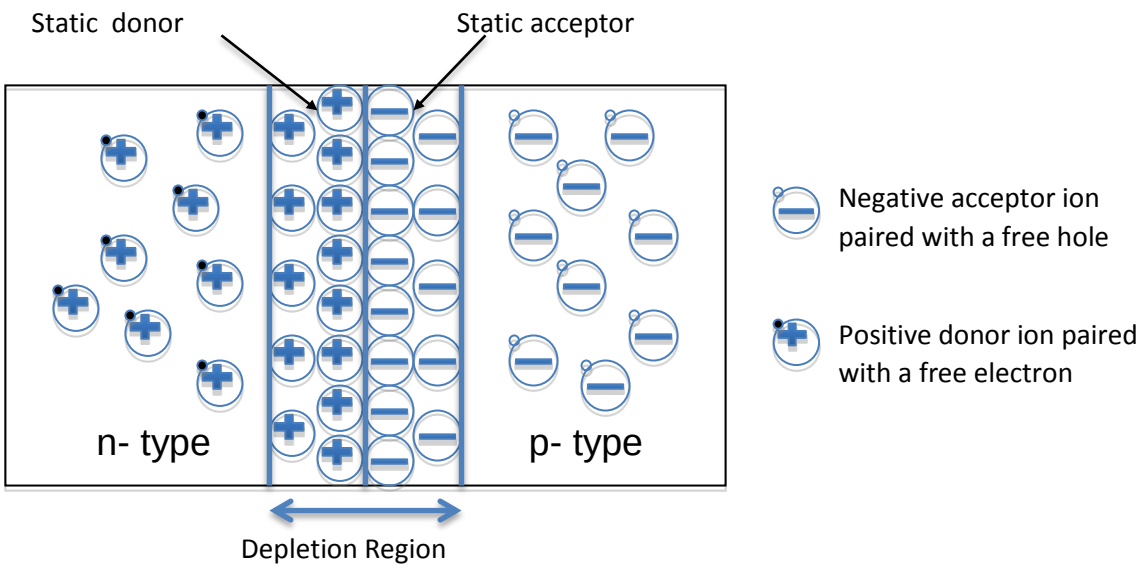

Figure 2.1 The schematic representation of a simple *p-n* junction with a depletion region formation

A *p-n* junction can act as a photovoltaic device. A *p-n* junction is formed by amalgamation of *n* and *p*-type semiconductors. Most commonly this is achieved using only one semiconductor, for example c-Si by doping the material suitably within the bulk of the material to form *p-n* homo-junction. The two semiconductors differ in that *n*-type semiconductors carry a majority of mobile (free) electrons shown together with a positive donor atom (doped by a V^{th} group atom) and the *p*-type semiconductors carry a majority of free holes (holes are vacancies created by electrons –carry unit positive

charge) shown together with a negative acceptor atoms (doped by a IIIrd group atom), maintaining electrical neutrality throughout the bulk crystal.

2.2 P-N Junction Principle

A classical *p-n* junction is shown above in figure 2.1. The device action starts with the formation of the junction. Since both sides of the junction have different concentrations of mobile charge carriers, diffusion starts across the junction. The on-going diffusion of charges leaves behind a region of oppositely charged fixed atoms i.e. electrons will diffuse from *n*-type semiconductor to the *p* side of the junction leaving behind positively charged fixed atom sites in the *n* side. Thus, as diffusion of holes and electrons proceeds, static charges build up both in the *p*-type and *n*-type materials close to the junction. This charged area is called the space charge region or the depletion region. This accumulation of oppositely charged regions gives rise to an electric field in the semiconductors close to the junction region. The electric field opposes the diffusion process. The two conflicting transfer process rates of drift (electric field induced) and diffusion give rise to a region around the junction, which is depleted of any free carriers and this region is left only with a sheath of positive donor and negatively charged acceptor atoms which will be immobilised and lead to an electric field and hence a potential across the junction. The electrostatic potential difference resulting from the junction formation is called the *built-in voltage*, V_{bi}.

2.3 Photovoltaic action

When photons carrying energy more than certain threshold energy (threshold energy being the band gap of the material on which the photon is incident) are incident on the material electrons are excited from valence band to the conduction band and electron hole pairs are created in the process. The charges get separated in the depletion region and accumulate at the terminals. This accumulation of charge at terminals gives rise to a potential difference which is called open circuit voltage (V_{oc}). Now when the two ends of the *p-n* junction are connected together without load, the resultant current is called short circuit current (I_{sc}). A more common parameter is the current per unit area or the current density (J), which will be used in later in the following chapters.

The open-circuit voltage, V_{oc}, is the maximum voltage available from a solar cell. The maximum voltage occurs when the total net current through the solar cell is zero. The open circuit voltage can be given by

$$V_{oc} = (nkT/ q) \ln (J_{sc}/ J_o + 1) \quad (2.1)$$

Where n, is the ideality factor,

K, is the Boltzmann constant

T, is the temperature

q, is the electronic charge

$J_{o,}$ is the dark saturation current density

J_{sc}, the short-circuit current density is the current per unit area through the solar cell when the voltage across the solar cell is zero. J_{sc} is the maximum obtainable current density from a solar cell and is achieved when the end contacts of the cell are short-circuited. In an ideal cell J_{sc} is equal to the photocurrent generated by the cell when exposed to light.

The fill factor (FF) is defined as the ratio of the maximum power from the solar cell to the product of V_{oc} and I_{sc}. The fill factor is a measure of the "squareness" of the J -V curve in forward bias. It is given by

$$FF = (V_{mpp} \times J_{mpp}) / (V_{oc} \times J_{sc}) \quad (2.2)$$

V_{mpp} and J_{mpp} are the voltage and current density values of the solar cell when the net Power (P_{mpp}) output of the cell is maximum.

Efficiency (η) is defined as the ratio of maximum power output from the solar cell to the incident illumination density P_{in}. It is typically measured at standard conditions of P_{in} 1000W/m^2, T= 298 K and AM 1.5 .it is given by

$$\eta = (V_{oc} \times J_{sc} \times FF) / P_{in} \quad (2.3)$$

Solar cells are analysed using J-V curves such as shown below. The general expression for the current produced by a solar cell is

$$J = J_{sc} - J_o(e^{qV/kT} - 1) \quad (2.4)$$

V_{oc} and J_{sc} are indicated in the figure 2.2. The area under the J-V curve is the power density, P obtainable (theoretical) from the solar cell. The maximum power obtainable is called the maximum power point (P_{mpp}).

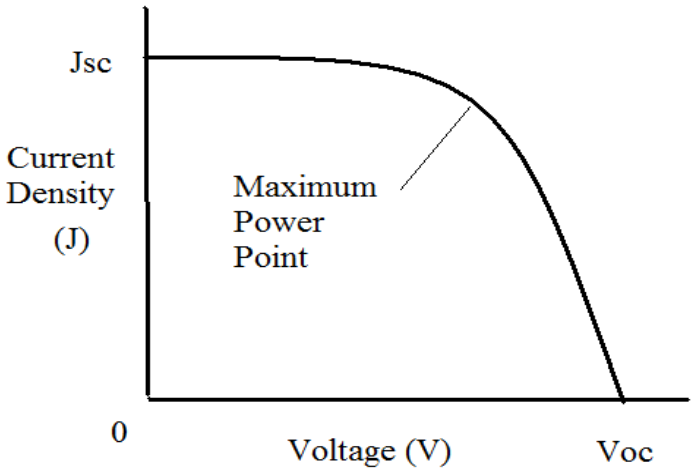

Figure 2.2 J-V curve of a typical solar cell when measured across a resistive load.

An equivalent circuit is usually used to depict a practical solar cell. The figure 2.3 below shows the equivalent circuit of a practical solar cell. Ideally a solar cell should have an infinite shunt resistance (R_{sh}) and zero series resistance (R_s). Unlike an ideal solar cell, R_s and R_{sh} are present in a practical solar cell. These two parasitic resistances R_{sh} and R_s impede the performance of a solar cell. Shunt resistance is caused due to imperfections in crystal structure of the materials. Shunt resistances are usually manifested as pinholes. Series resistance is the resistance of the bulk of the materials as well as the resistance at the contacts.

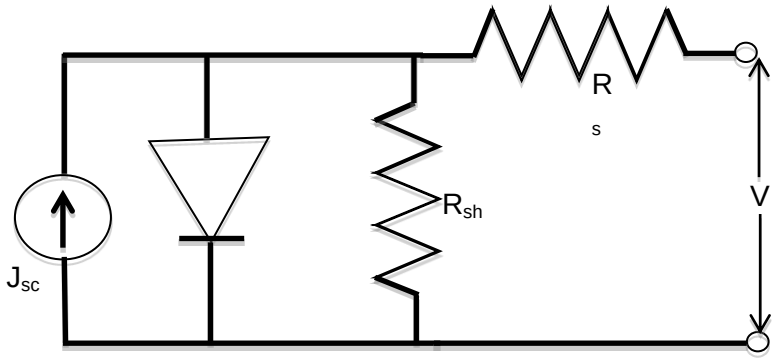

Figure 2.3 Equivalent circuit representation of a non-ideal solar cell

2.4 Cadmium Telluride

CdTe [13-18] is a II-VI compound with a direct band gap 1.45 eV with semiconducting properties making it one of the most potential solar cell materials. The n and p-type doping is controlled by the relative vacancies of Cd or Te atoms. The ease of process, generally vapour transport and close space sublimation to obtain both CdTe and CdS layers make it best among all PV technologies in terms of payback time.

2.4.1 Properties of CdTe

CdTe is an optimum material to be used as absorber layer in thin film solar cells because of its properties: CdTe has an energy gap of 1.45 eV, very well suited to absorb the solar light spectrum. The absorption coefficient for CdTe in the visible light range is $> 10^5$ cm^{-1} [19]. Also the band gap between conduction and valence levels in CdTe is direct. In effect even a small thickness of cadmium telluride ~ 1 μm is sufficient to absorb majority of photons from incident light.

A variety of methods can be used to prepare CdTe. The advantage of CdTe lies in that as- deposited films made from different methods are similar in structure and electronic properties. CdTe predominantly exists in zinc blende structure. Each Cd atom is tetrahedrally surrounded by four Te atoms and vice versa. The predominant orientations observed for CdTe thin films are the (111) and (110) orientations. The typical unit cell dimension is 6.481 Å and CdTe bond length is 2.806 Å [19].

2.4.2 Deposition methods for CdTe

CdTe forms stoichiometric films when heated sufficiently typically above 600^{o}C. The most common CdTe film deposition method is high vacuum deposition; CdTe is evaporated from a heated crucible and condensed on a substrate positioned in front of this crucible inside a vacuum vessel. The crucible and source material are kept at a temperature around 700^{o}C, and the substrate is heated to temperatures between 200^{o}C and 400^{o}C.

(a) Physical vapour deposition

In this form of deposition vapours of Cd and Te exist in equilibrium with CdTe solid which deposits on the substrate. Either elemental cadmium and tellurium or CdTe compound can be used as source for Cd and Te_2 vapours. Source temperature, source to substrate distance and total pressure are crucial parameters in this type of deposition. The source temperature is between 700- 900^{o}C while the pressure is around 10^{-6} Torr [18].

(b) Close-spaced sublimation (CSS)

A modified version of PVD is CSS where substrate is maintained at temperatures close to 500^{o}C. The evaporation source is made in the form of a flat plate essentially the same size as the substrate and is placed in close distance (typically 2-3 mm) in front of the

source. The source, CdTe powder is placed in a graphite boat. Thermocouples are used to monitor and control the temperature. Tungsten lamps may be used to heat the source and the substrate. Both the source and the substrate should be heated independently of each other. An insulator is provided between source and substrate. An inert gas such as N_2, Ar or He is used as ambient at pressures of 1mbar or higher. Source temperature, substrate temperature, source/substrate spacing and pressure are important parameters. The CSS method has yielded the highest small area efficiency [19-28].

(c) Vapour Transport Deposition

In CSS, vapour transfer occurs by diffusion. In VTD vapour transfer is by convection using a carrier gas. It involves moving substrates, which allows higher deposition rate. A vapour is saturated with Cd and Te, which delivers the gases to the substrate. The substrate is maintained at a cooler temperature where CdTe gets deposited. The carrier gas flow rate can be controlled which controls the deposition rate [29].

(d) Sputtering

CdTe films can also be deposited by radio-frequency magnetron sputtering from compound targets. This process is carried out in a vacuum ambient at pressures around 10 mTorr. In this process, an inert gas such as Ar is used as ambient. Under high vacuum plasma conditions are created by applying an electric field. As a result of the electric field Ar atoms are bombarded onto CdTe targets. Cd and Te atoms are then sputtered and condense on substrate. The sputtering process is typically a low temperature method with temperatures around 300 ^{o}C. The method allows good process control [30]. Deposition rates are typically about 100 nm/min.

(e) Spray Pyrolysis /chemical spraying

Spray pyrolysis involves the atomization of the precursor solution, spray formation followed by the chemical reaction on a hot substrate. An aerosol precursor solution is prepared. The solution contains heat decomposable compounds of cadmium and tellurium. The solution is then sprayed onto a hot substrate. The substrate is usually maintained at a temperature of about 500 ^{o} C. The pH, concentration and quantity of the solution are important parameters as is substrate temperature. Other parameters that affect film property are spray rate, nozzle to substrate distance and nozzle diameter. It is a non-vacuum technique [31].

(f) Electrodeposition

Electrodeposition of CdTe consists of the galvanic reduction of Cd and Te from Cd^{2+} and Te^{+} ions in acidic aqueous or non-aqueous electrolytes. The typical setup contains a container filled with a solution containing cadmium and tellurium ions. Two (or three) electrodes are immersed into the solution. The cathode is the typically glass/ TCO/CdS stack. The counter electrode is an inert metal electrode such as platinum.

A reference electrode is also required which determines the deposition potential of CdTe with respect to a standard electrode (Ag/AgCl standard electrode or Standard Calomel Electrode, SCE). Potentiostatic or galvanostatic conditions can be used to deposit CdTe layers. As-deposited films can be fabricated as stoichiometric CdTe, Te-rich (by increasing Te species concentration in the bath) or Cd rich (by depositing at low potentials with limited Te species concentration) [32].

(g) Metal Organic Chemical vapour deposition

In this technique organic compounds of cadmium and tellurium are used as source with a suitable carrier gas. A metal organic chemical vapour deposition (MOCVD) system typically consists of a gas control system and a reaction tube. Common Cd and Te precursors are dimethylcadmium and diisopropyltellurium. Substrates are maintained at temperatures around 200-400^{o}C. A carrier gas like nitrogen carries the vapours to reaction tube. Flow rate of nitrogen is controlled which in turn controls the reaction mixture composition near the substrate. The process does not require vacuum [33].

(h) Screen Printing

In this simple technique, Cd, Te and $CdCl_2$ are combined together in the form of a paste and applied to the substrate through a screen. A pattern is photographically defined on a stainless steel screen. Screen printing depends on some important parameters such as: the viscosity of the paste, the mesh number of the screen (number of meshes per inch), and the pressure and speed of the squeegee. The printed film is dried and then heated to facilitate recrystallisation of CdTe layer [34].

2.4.3 CdTe Solar Cells

The CdTe solar cells can be grown in both substrate and superstrate configurations. The CdTe/CdS layers for superstrate cells are grown on transparent conducting oxide (TCO)-coated glass substrates. The glass substrate can be alkali-free glass for high-temperature processes (500-600^{o}C) or a low-cost soda-lime glass for growth process temperature below 500^{o}C. Although both superstrate and substrate structures have been

tried for CdTe solar cells, better results have been achieved for superstrate structure [35]. For flexible solar cells, substrate configuration is most suited because it does not have to be transparent that allows different types of foils such as stainless steel, polyamide, molybdenum for the growth of the flexible cells [36]. Both the substrate and superstrate structures are shown in figure 2.4 (a) and (b) respectively.

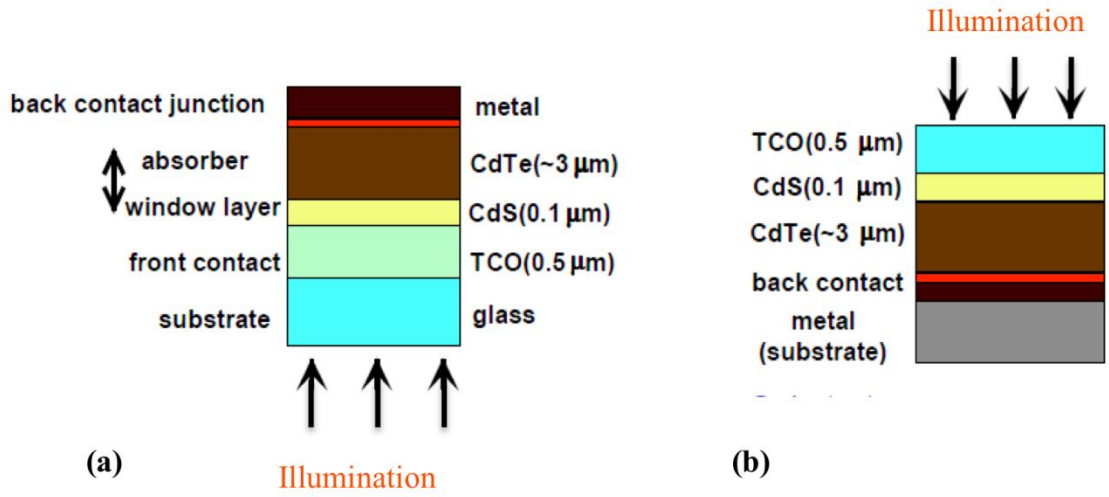

Figure 2.4 Superstrate (a) and substrate (b) configuration of CdTe solar cell stack [37]. Arrows indicate the direction of the sun rays.

The basic *p-n* diode junction in a CdTe based solar cell is formed between p-type CdTe absorber layer and n-type CdS window layer. The superstrate structure stack typically used for a CdTe based thin film solar cell is shown in figure 2.4. The various layers are discussed below.

(a) Transparent Conducting Oxide

The glass layer is coated with conducting oxides such as SnO_2 (tin oxide) or indium doped tin oxide or fluorine doped tin oxide or cadmium stannate. This layer is transparent and acts as the front contact. A highly transparent and conducting TCO layer is used to form an Ohmic contact with the CdS. F-doped SnO_x [SnO_x:F (FTO)] or ITO are the most commonly used TCOs for CdTe solar cell. Intrinsic SnO_x layer between CdS layer and TCO layer are used that prevents shunts through pinholes in CdS [19].

(b) CdS – Window layer

As mentioned earlier, cadmium sulphide is the preferred heterojunction partner with CdTe. Cadmium Sulphide (CdS) exists in two crystalline forms namely zinc blende and wurtzite structure with alternating Cd and S atoms. Each Cd atom is surrounded by four

S atoms in a hexagonal close packed structure. The S vacancies act as donors and make the CdS n-type. CdS has a wider band gap of 2.42 eV and allows most of the incident light photons to pass through and enter the CdTe absorber layer more readily. To minimise absorption in the window (CdS) layer it is very thin – in the range of 200 to 500 nm or even thinner. Like CdTe, CdS forms stoichiometric films easily and by similar methods as used for CdTe deposition. CdS layer is deposited on top of the TCO layer. Because the CdTe and CdS are mixed easily during the cell fabrication process, it leads to the formation of interfacial layer of $CdS_{1-x}Te_x$ [38] and in effect a high quality and efficient CdTe/CdS junction is formed. Sometimes a high resistance layer is included between TCO and CdS. CdS can be deposited by a variety of processes such as sputtering, chemical bath deposition, CSS, electrodeposition, spraying, and screen printing. The processes and process conditions used are similar to those for CdTe deposition. This allows for increased compatibility between CdS and CdTe layers during manufacturing.

(c) CdTe - Absorber layer

The CdTe is deposited directly on top of CdS to form the *p-n* junction by any of the methods described in the previous chapter. All methods result in polycrystalline nature in as-deposited films. Typical CdTe layer thicknesses range from 3-5µm. It has been observed that post deposition heat treatment particularly in the presence of Cl^- species improves CdS/CdTe junction interface, surface morphology of bulk CdTe and electrical properties of the solar cell. $CdCl_2$ is used for this treatment [19]. The $CdCl_2$ treatment can be solution based (where the CdTe layer is dipped in cadmium chloride – methanol solution) or vapour based (where CdTe is exposed to $CdCl_2$ vapour in a closed chamber). The CdTe substrate after treating it with $CdCl_2$ is heated to temperatures between 350- 420 ^oC for 15-30 min.

(d) Back contact

Under the superstrate structure, p type CdTe needs to be contacted to a metal conductor to form an Ohmic back contact. A p type semiconductor requires a metal with high work function to form an Ohmic contact. CdTe forms a Schottky barrier with most metal back contacts [39]. To overcome this problem researchers use buffer layers to make the surface of CdTe a p^+ rich surface. A variety of buffer layers are used for this purpose. A few chemical techniques such as the bromine- methanol etch or nitric-phosphoric acid etch may also be used. Dry treatment processes include exposure to ion beam under vacuum conditions [19].

Chapter 3: CdTe Thin Film Preparation and Characterisation

3.1. Introduction

This chapter describes the electrodeposition method used for CdTe thin film preparation, its characterisation and analysis. Details of the CdTe thin film growth techniques are presented in this chapter. The experimental details of thin film characterisation are described. Methods such as XRD (X –Ray Diffraction) and SEM (Scanning Electron Microscopy), have been used to characterise the thin films.

3.2 Electrodeposition

Electrodeposition is a very promising and well established industrial method which can be used to deposit thin film semiconductor materials to be used in a range of devices including solar cells. There are a number of key advantages of the electrodeposition technique. It is simple, fast, can be used for the synthesis of multinary precursors for subsequent processing and most importantly it is easy to scale-up for commercial applications [40]. Figure 3.1 shows a schematic diagram of the electrodeposition system for the deposition of thin films used in this study.

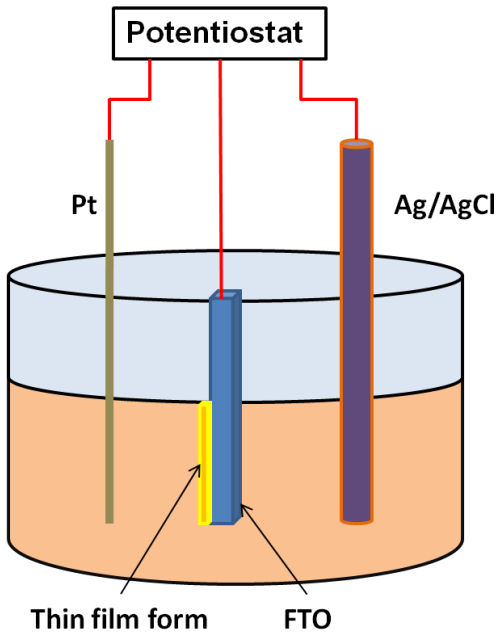

Figure 3.1 Schematic diagram of the electrodeposition set up used in this study. The sample is connected to the working electrode, and a Platinum counter electrode and an appropriate reference electrode (i.e. Ag/AgCl electrode) have been employed.

A typical electrolytic solution (used in the electrodeposition) contains positively charged (cations) and negatively charged ions (anions). Under the applied external

electric field, the cations migrate to the cathode where they are discharged and deposited as a thin film. In practical electrodeposition processes, the chemical reaction around the electrode area occurs in a more complicated way than that shown in figure 3.2. Under the influence of an applied potential, rearrangement of ions near the electrode surface results in an electrical double layer called the Helmholtz double layer, followed by the formation of a diffuse layer as shown in figure 3.2. These two layers are referred to as the Gouy-Chapman layer.

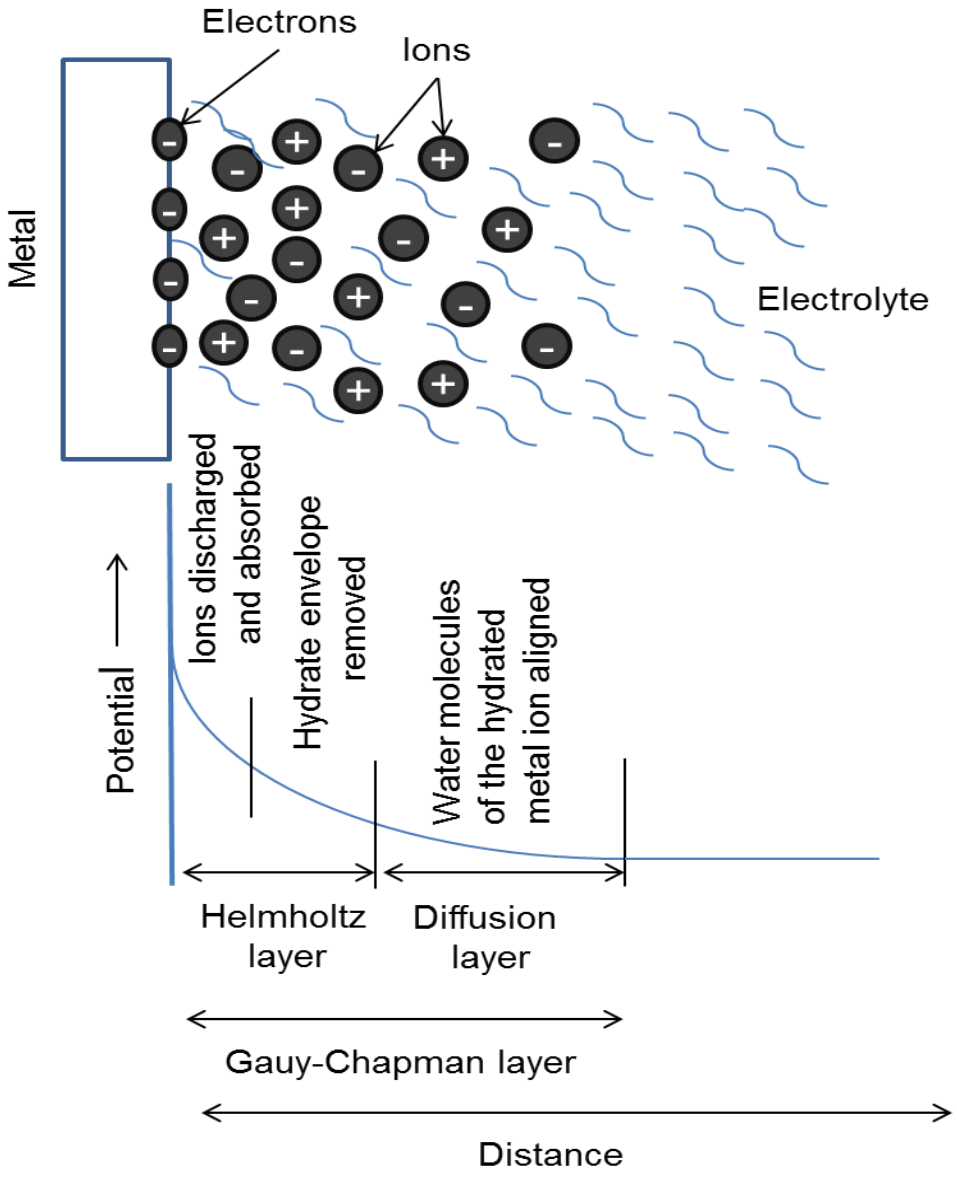

Figure 3.2 The influence of an applied potential, rearrangement of ions near the electrode surface results in an electrical double layer called the Helmholtz double layer, followed by the formation of a diffuse layer.

The process can be explained as follows:

- Migration: The hydrated metal ions in the solution migrate towards the cathode under the influence of impressed current as well as by diffusion and convection.
- Electron transfer: At the cathode surface, a hydrated metal ion enters the diffuse double layer, where the water molecules of the hydrated ion are aligned. Then the metal ion enters the Helmholtz double layer where it is deprived of its hydrate envelope.

- The dehydrated ion is neutralized and adsorbed onto the cathode surface.
  - The adsorbed atom then migrates or diffuses to the nucleation point where the growth starts on the cathode surface.

The thickness of the electrodeposited layer on the substrate is determined by the duration of the electrodeposition and also the current density.

Electrodeposition has the advantages that the technique is inexpensive; it uses the raw materials more effectively and can be used for large scale production. It is a non-vacuum deposition method with low temperature growth. It allows great control of deposition thickness of the film.

3.3 CdTe Thin film Preparation

The preparation of CdTe thin films can be done by electrodeposition technique. The electrodeposition of CdTe thin film has been done on glass/FTO substrates. The CdTe film can be grown on glass/ FTO surface at room temperature of 25°C using aqueous solution. The FTO glass substrate was first properly cleaned with soap water and dried with the nitrogen gas so as to remove any impurities on the substrate. The aqueous electrolytic solution containing $CdSO_4$ and TeO_2 was used for deposition. The chemical composition and specification is given below in the table 3.1. All chemicals used were analytical reagent grade of purity more than 99.9%. A standard three-electrode system was used with Ag/AgCl electrode as a reference electrode, glass/FTO as working electrode and platinum as counter electrode. All three electrodes were plunged into the electrolytic aqueous solution containing cadmium and tellurium salts.

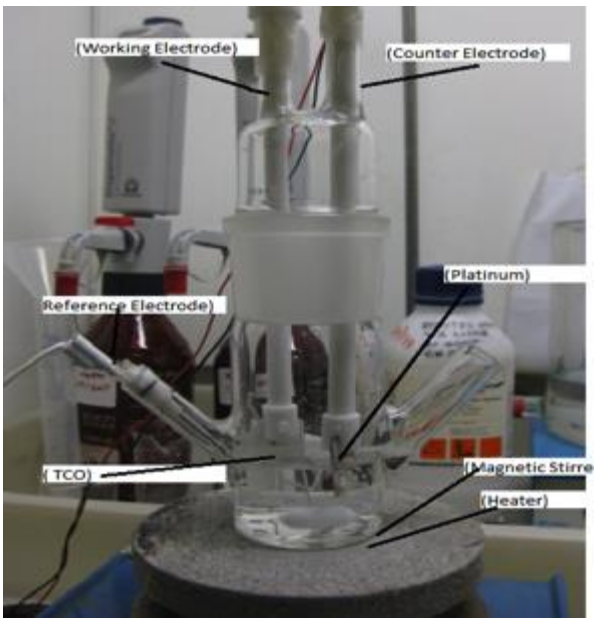

Figure 3.3 A photograph of the apparatus used for the electrodeposition.

Process Parameters	**Electrolytic Bath** $CdSO_4$-TeO_2
Temperature	25°C
Stirring rate	600 rpm
Concentration	Molarity- 1 M- Cd Molarity- 10^{-3}M-Te
pH (using H_2SO_4)	2
Potential range	0.3-0.5 V
Current density	200-600 µA/cm^2
Typical Thickness	1 µm
Cell Area	1.5 cm^2
Deposition Time	2 hours on FTO substrate

Table 3.1 Experimental conditions used to prepare CdTe thin films

The electrodes were supplied with a constant deposition potential using the PARSTAT 2273 system. PARSTAT 2273 uses the Power CORR software. This software allows us to keep the potential of the electrochemical system constant at the desired value and plot the resulting I vs T (current versus time) graphs. Galvanostatic and potentostatic measurements were carried out at different levels of current and voltages. Different potential ranges were tried to deposit the film during potentostatic operation ranging from -0.6 V to -0.3 V. The solution was stirred continuously so as to maintain the

uniformity of the films. Different stirring rates were tried but the best deposition was found out at the stirring rate of 600 rpm. Sulphuric acid (H_2SO_4) was used to maintain the pH of the solution in between 2- 6 so as to dissolve the TeO_2 ions. The deposition was done for 2 hours. The CdTe film of thickness of ~1 μm was deposited. The area of deposition was 4 cm^2.

The deposition current (I) response of the system to the input fixed deposition potential was similar for each value of potential. After a few minutes the current stabilised at an equilibrium value and stayed at that value for the entire deposition. The table 3.2 for obtained charging current at different potential is given below.

Parameters	**Samples of CdTe**			
Deposition Potential (V)	-0.3	-0.4	-0.5	-0.6
Charging Current (μA)	450	500	100	250

Table 3.2 Current responses to fixed deposition potentials

3.4 Materials and device characterisation

X-ray diffraction (XRD), Scanning Elecron Microscopy (SEM), Energy Dispersive X-ray Spectroscopy (EDS) and DC conductivity measurements were carried out on the CdTe films deposited on glass/FTO and glass/FTO/CdS surfaces. The Brucker D8 (Copper X-ray) 1.542 Armstrong (Std.) was used for XRD characterisation, Leo (Carl Zeiss) 1530 VP machine for SEM analysis and Energy Dispersive Analysis by X-rays (EDAX) measurements machine for EDS measurements (Energy Dispersive X Ray Spectroscopy).

3.4.1 Structural Characterisation

X-ray diffraction (XRD) measurements were carried out on the plain CdS deposited sample and CdTe deposited sample to examine the structural characteristics of the sample. The corresponding X-ray Diffractograms of the samples are given in the figure 3.4 below. The XRD pattern for as-deposited CdTe films reveals that the deposited

films are polycrystalline in nature. The two dominant peaks were observed at (111), (220). A smaller peak is observed at 33.8^{o} that may be due to underlying SnO_2 layer onto which as-deposited CdTe films are prepared, showing multiple peaks.

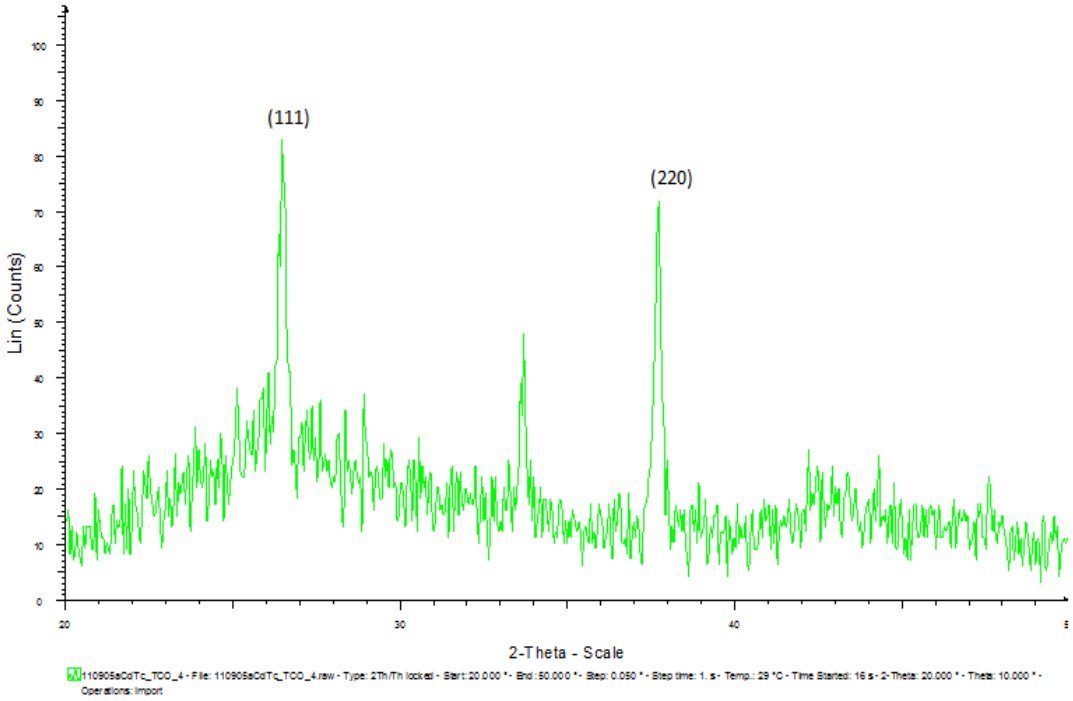

Figure 3.4 XRD pattern of as-deposited CdTe using electrodeposition

3.4.2 Surface Morphology

Scanning electron microscopy (SEM) tests were conducted to investigate the surface morphology of the CdTe deposited sample using TeO_2. Before SEM, the samples were coated with gold by sputtering for 30 sec with the current of 20 mA to make the samples more conducting. The figure 3.5 shows good adherence or interface between as-deposited CdTe and FTO. The typical grain size was approximately 250 nm. Uniform and smooth crack free surface was obtained from the morphology results as predicted from the previous results with spherical shaped grain spread all over the film of both the samples. The typical cross section image of the film is shown in the figure 3.5 below. The SEM indicates two layers within the CdTe layer – one of which seems to be CdO layer.

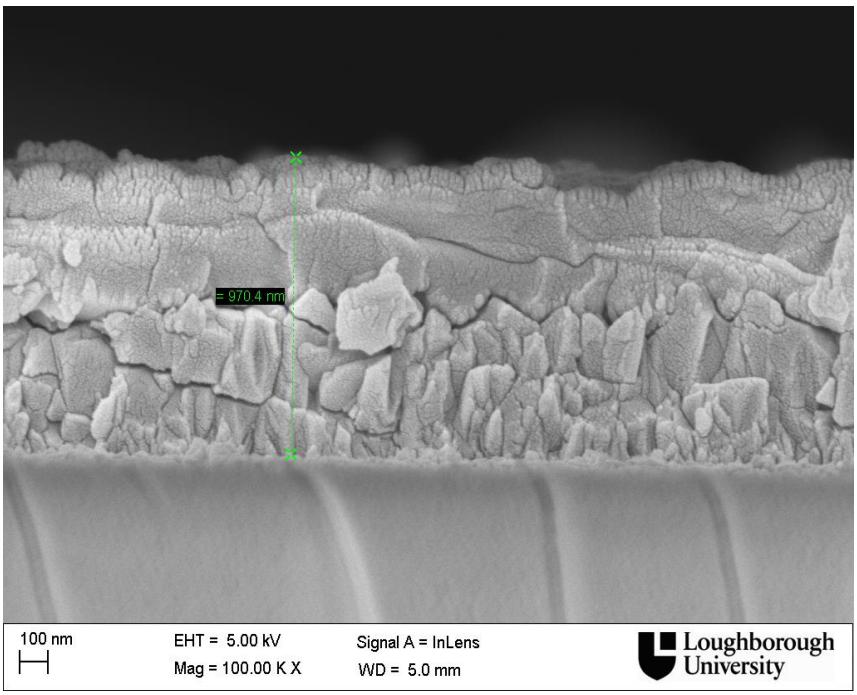

Figure 3.5 Cross section view of CdTe thin film on FTO/Glass

The SEM front view image of the film is given in the figure 3.6 below which also show the uniform grain size deposited all over the film.

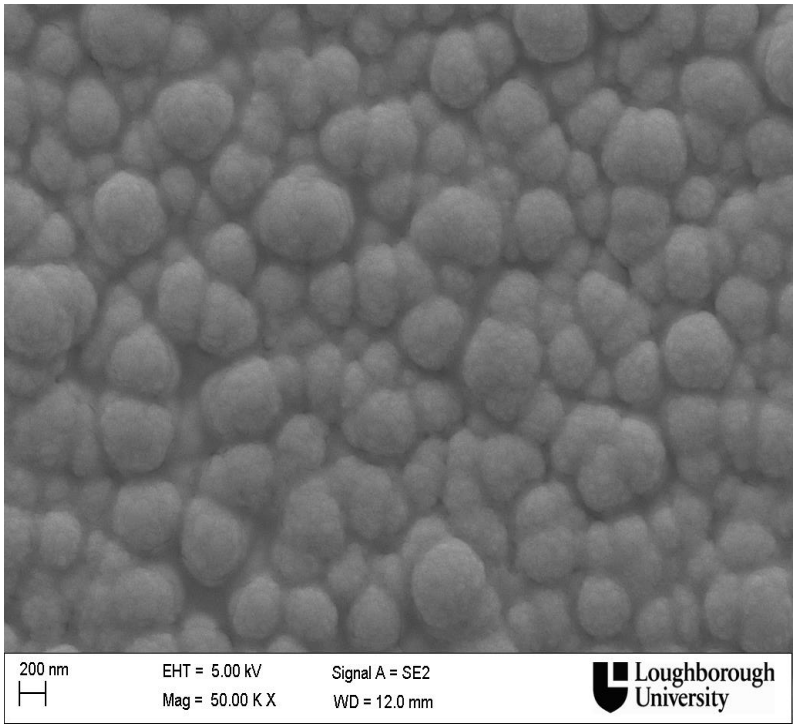

Figure 3.6 Scanning Electron Microscopy (SEM) image of CdTe thin film

3.4.3 EDS Data Analysis

Figure 3.7 shows typical EDS data on CdTe films deposited. The observed peak patterns are shown. The table 3.3 shows the atomic percentage of Cadmium and Tellurium on the deposited films. The samples were Tellurium rich which was obtained by managing the deposition current densities. It has been suggested [41] that by controlling the deposition conditions, a tellurium rich and hence a *p* type CdTe film can be deposited. High oxygen content may be due to CdO layer getting formed and Sulphur may be appearing due to additives such as sulphuric acid.

Element	Wt %	At %
Carbon (C)	1.06	8.10
Oxygen (O)	1.99	11.43
Silicon (Si)	0.38	1.26
Sulphur (S)	2.84	8.15
Cadmium (Cd)	35.67	29.20
Tellurium (Te)	58.06	41.86
Total	100.00	100.00

Table 3.3 Atomic percentages of elements in CdTe film using EDS data

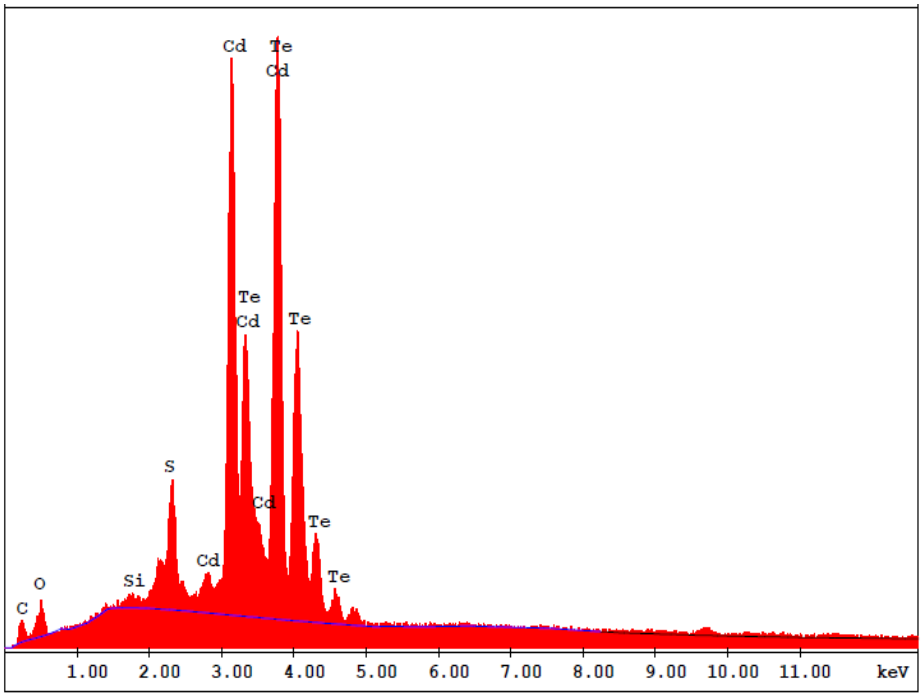

Figure 3.7 A typical EDS spectra of CdTe thin film

3.5 Conclusion

The electrodeposited CdTe film is uniform in nature with good thickness. The deposition conditions need to be optimised to show better morphology. The electrodeposited layer was not used for ultra-thin film solar cells. The experiment demonstrates a simple method to deposit CdTe films on conducting substrates (here FTO/glass). The CdTe thin films prepared from the electrodeposition were not used in the device due to its stoichiometry. This work needs more optimisation to make the stoichiometric CdTe films which leads to device fabrication. A future plan requires the optimisation of CdTe stoichiometric layers restricting CdO (possible source of oxygen) layers and substantial impurities of Sulphur arising from H_2SO_4 additive. This will be carried out in tune with CdTe solar cells results of various thicknesses prepared using MOCVD method in collaboration with Glyndŵr University.

Chapter 4: Preparation and Characterisation of Ultra-thin CdTe Solar Cells

4.1 Introduction

In order to testify the theoretical simulation results, CdTe thin films were prepared by MOCVD method. The ultra-thin CdTe films were used to form CdTe solar cell stack. This chapter summarises the results obtained from CBD-CdS/MOCVD-CdTe devices using different thicknesses with Au back contacts using only front (junction side) illumination. CBD-CdS/MOCVD-CdTe devices were also produced for optical modelling study of CdTe devices for window glazing purposes. CBD-grown CdS on NSG TEC A7 samples were used as substrates for devices to be produced by Dr. A. Clayton at the Centre for Solar Energy Research (CSER) at Glyndŵr University, using the MOCVD process to deposit CdTe with thicknesses ranging from 1000 – 300 nm [45].

4.2 Experiment Procedures

4.2.1 Chemical bath deposition for CdS

Chemical bath deposition is a simple technique for the deposition of CdS on glass substrate. The substrate was Pilkington TEC7 glass (FTO/glass). The aqueous solution contained 200 ml of water, 15 ml of 0.014M Cd $(CH_3COO)_2$, 10 ml of 0.055 M thiourea and 25 ml of 0.5 M NH_4OH. All chemicals used are 99.99% pure and dissolved in deionised water. To maintain the suitable pH of the solution, the solution of 0.5 M ammonia was used. The temperature of the deposition was maintained at 70°C and the solution was stirred continuously so as to maintain the uniformity of the CdS film and deposition time was between 20 min and one hour. After the completion of deposition, the deposited film was washed with warm water and dried using the nitrogen gas. In order to increase the electrical conductivity of the deposited CdS film, annealing treatment was done at 450°C for 15 minutes. CdS films of thicknesses between 60 nm and 250 nm were deposited using this process. The thickness of CdS films was measured using a Dektak profilometer.

4.22 MOCVD deposition of CdTe at CSER

Substrates (Glass/FTO/CdS) were cut to size giving devices approximately 2 x 2 cm^2 in area, and were prepared using a methanol swab / N_2 blow dry before being loaded into the chamber. CdTe deposition was carried out in a horizontal furnace tube with H_2 as the carrier gas. The growth temperatures were varied between 200^oC and 420^oC. The precursors for Cd and Te were dimethylcadmium and diisopropyltelluride, respectively. Arsenic was used as a dopant to improve the contact between CdTe and gold back contact. $CdCl_2$ treatment was carried out in the reaction chamber in situ. Tertiary butyl chloride was used as a precursor for Cl used in the $CdCl_2$ treatment. An in situ triple wavelength laser reflectometer was used to monitor the growing layer thickness. After the CdTe deposition and $CdCl_2$ treatment, the solar cell device samples were completed with thermally evaporated 0.25 cm^2 gold back contacts. To make the front contact the CdS and CdTe layers were removed in order to expose the FTO. A Ga/ In paste was then applied to the FTO to make the contact. Removal of the layers to expose the FTO layers was extremely difficult. The most effective way to accomplish this was to use a cocktail stick dipped in concentrated Br/ methanol solution to scrape along the edges of the device where the front contact was to be made.

4.3 Results and Discussions

4.3.1 Device Characterisations

The *J-V* measurements were carried out with only front (junction-side) illumination under AM1.5 using an Abet Technologies Ltd. solar simulator with light power density output equal to 1000 W/ m^2 calibrated with a Fraunhofer a-Si reference cell. The *J -V* curve for the CdTe (400nm)/ CdS (60nm) device is given in figure 4.1. The results for each device are shown in table 4.1.

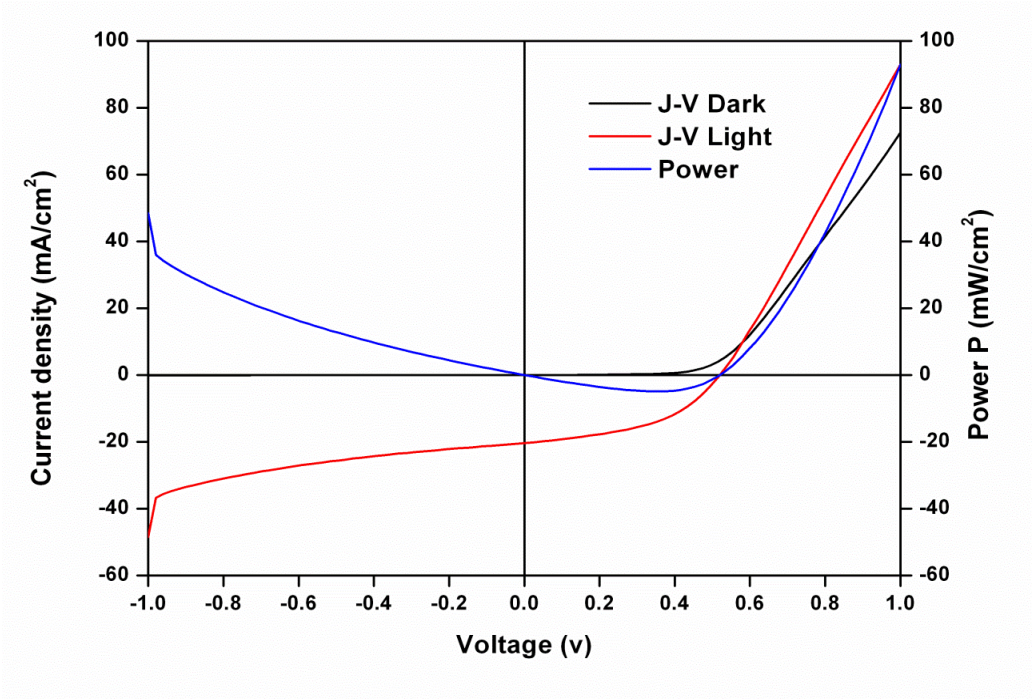

Figure 4.1 J-V curve of CdTe solar cells with gold back contact of 400nm CdTe and 60nm CdS thin film.

Each device has been labelled using the system at CSER. Device 324 did not perform well, most likely due to insufficient removal of the CdS layer from the FTO when making the front contact. This was supported by the high series resistance (R_s) shown in table 4.1. The large shunting effect resulting in low values for shunt resistance (R_{sh}) will also have had a detrimental effect on device PV performance. In general, all devices were characterised with high R_s and low R_{sh}.

Device	Description	Substrate	Cells	I/V	Eff (%)	Jsc (mA/cm²)	Voc (mV)	FF (%)	Rs (Ω cm²)	Rsh (Ω cm²)
CSER 324	1000nm MOCVD-CdTe on 250nm CBD-CdS	NSG TEC A7	4	Best	0.3	9.5	121	24.9	11.4	18.7
				Mean	0.1	6.2	86	24.2	15.4	15.5
				σ	0.1	2.3	25.2	0.6	3.5	3.6
CSER 325	600nm MOCVD-CdTe on 250nm CBD-CdS	NSG TEC A7	6	Best	6.2	20.0	566	59.6	3.2	233
				Mean	4.6	18.5	465	48.5	4.5	145
				σ	2.3	0.4	199.0	16.1	0.8	99
CSER 326	500nm MOCVD-CdTe on 60nm CBD-CdS	NSG TEC A7	6	Best	6.8	21.6	566	56.3	5.8	202
				Mean	4.9	21.0	505	45.2	7.2	99
				σ	1.6	0.4	75.5	9.4	1.9	62
CSER 327	400nm MOCVD-CdTe on 60nm CBD-CdS	NSG TEC A7	4	Best	4.9	21.2	525	45.4	6.4	65
				Mean	3.9	20.3	460	40.3	5.3	48
				σ	1.2	0.8	68.5	6.1	1.3	20
CSER 328	300nm MOCVD-CdTe on 60nm CBD-CdS	NSG TEC A7	2	Best	4.1	18.0	505	45.2	6.6	77
				Mean	2.4	16.8	334	35.8	7.5	44
				σ	2.4	1.7	242.5	13.4	1.3	47

Table 4.1 Device and electrical parameters of ultra-thin CdTe/CdS solar cells [45]

However, *J-V* results for devices 325 – 328 for CdTe thicknesses ranging from 600 – 300 nm were promising even with the resistance effects. The short circuit current (J_{sc}) for device 326 is improved relative to device 325 due to the thinner CdS window layer, which allows more high energy photons to transmit through to the CdTe absorber layer. This results in a greater efficiency for device 326 in comparison to device 325, which has a thicker CdTe absorber layer. The V_{oc}, J_{sc} and FF drop coincided with a reduction in absorber thickness from 600 to 300 nm. This is due to an increase in lateral non-uniformities across the device coupled with an increase in the density of pinholes leading to micro-shunts. The fall in mean R_{sh} as the CdTe thickness reduces supports this. Further, the drop in J_{sc} with respect to the decrease in the absorber thickness appears also consistent with the fact that less photons will get absorbed as the thickness of the CdTe absorber is reduced.

4.3.2. Optical and Spectral response

External quantum efficiency (EQE) measurements were carried out using a Bentham spectral response spectrometer under unbiased conditions over the spectral range 300 – 1000 nm. Figure 4.2 below shows EQE curves for the cells with highest efficiency from devices 325 to 328.

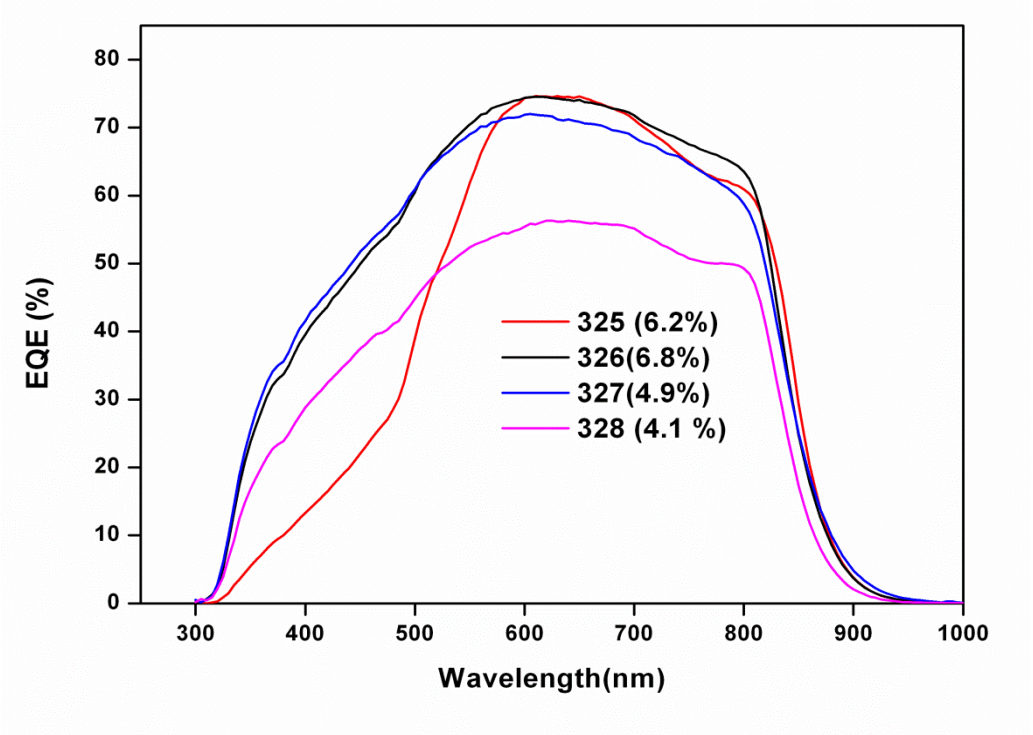

Figure 4.2 Spectral responses of CdS/CdTe solar cells from devices 325 to 328 showing efficiency for each individual cell measured.

The EQE curves clearly show the benefit of having a 60 nm CdS window layer compared to CdS 250 nm in thickness. The devices with thinner CdS have improved response in the blue region of the solar spectrum, correlating with the observed increased J_{sc} for devices 326 and 327 in comparison with device 325. The EQE curves show a decreasing slope towards the longer wavelengths approaching the CdTe band edge relating to the optical limitations of the ultra-thin CdTe absorber layer thicknesses. This decrease may be due to the reduction in the diffusion length of the carriers, which is due to the recombination occurring at the grain boundaries of the bulk absorber CdTe. A general decease in EQE over the CdTe photoactive region is observed as the absorber thickness is reduced. This could be related to the increased shunting due to greater influence from lateral non-uniformities.

4.4 Conclusions

Ultra-thin CdTe/CdS solar cells were prepared using MOCVD process for CdTe layer and chemical bath deposition for CdS. Efficiencies of 6.8 % for 600 nm and 4.9 % for 400 nm CdTe thickness were observed. Even 300 nm thick CdTe cells showed efficiency greater than 4%, though cells suffered from low shunt and high series resistance resulting in a reduced fill-factor. Use of alternative TCO is expected to yield better results as studied in [43]. The TEC7, FTO used from NSG-Pilkington group, which is processed on a float glass under atmospheric spray deposition of precursors suffers from a surface undulation of around 200nm which may be a factor adding to the shunt loss effects at considerably low thickness of the absorbers such as 300nm used in the studies.

Chapter 5: Optical Modelling of CdTe Solar Cell Stack

5.1 Introduction

CdTe is a proven absorber material in solar cells. Due to its optimum band gap and high absorption coefficient a CdTe layer of thickness less than 1 micron is semi-transparent but still has the potential to absorb over 90% of incident photons. This property of CdTe can be utilised in ultra-thin film solar cells. A thin film photovoltaic layer if applied on a conducting glass sheet (glass coated with TCO), the glass system can act as a window in buildings as well as generate power. If optimised properly, a double glazed window layer coated with the thin photovoltaic film can generate power along with reducing unwanted solar gains (i.e. a part of the energy is absorbed by the cell material, while the overheating during summertime can be avoided, especially in hot countries). However, to achieve this precise control over the thickness of layers is crucial to optimise absorber efficiency along with optical transparency.

This chapter summarises the optical design and experimental work that was carried out to study the possibility of a device as explained above and to optimise the transparency, and power generation of the photovoltaic stack.

To carry out the study, the following methodology was used

i. Input complex refractive index (n, k) values of individual layers comprised in the solar cell stack, using experimental ellipsometric data conducted on each layer separately.
ii. Generate optical spectra of individual layers using CODE software, compare with experimental spectra and derive a close fit computer model for each layer.
iii. Stack up the layers one on top of each other and simulate their optical (transmittance) and electrical (photocurrent) properties using the program.
iv. Investigate how variation of CdS and CdTe layer will affect the transmittance of the stack as well as the photocurrent generated.
v. Compare modelled data to experimental results.

5.2 Theoretical Background

The various phenomena that occur when light (an electromagnetic wave) interacts with a solid are refraction and absorption [44] occurring inside the solid. The rest of the incident light is either reflected back from various surfaces of the solid or is transmitted out. The propagation of the beam through a transparent medium is described by the refractive index n. This is defined as the ratio of the velocity of light in free space c to the velocity of light in the medium *v*. The absorption of light by an optical medium is quantified by its absorption coefficient, α. The absorption and refraction of the medium can be described a single quantity called the complex refractive index. The dielectric function or the refractive index of a thin film represents connection between the internal physical mechanisms (electronic, atomic and free charge carrier oscillations) in the bulk of a material to the incident electric field.

The complex refractive index, n_c is given by

$$n_c = n + ik$$

Where, n = refractive index, k = extinction coefficient = $\lambda\alpha/ 4\pi$, λ = incident light wavelength, α = absorption coefficient, i = complex imaginary unit

The optical properties of any material or thin film can be completely defined by its n and k values. Once the n and k values are known in the desired wavelength region, reflectance and transmittance spectra of the thin films can be calculated. To obtain n and k values, ellipsometric measurements were used. Each component layer of the stack was deposited separately on plain float glass under the same operating conditions as were used for depositing the layers in the solar cell. Three different incidence angles were used for each coating/ thin film on glass to obtain the n, k values. The n, k values were in the wavelength range from 250- 2500 nm. The obtained values were fed into the CODE software. This software uses mathematical functions to compute and simulate properties of thin films such as transmittance, reflectance etc using only n, k values. For the individual layers, standard formulae available in the CODE program were used to generate first approximation results of transmittance. CODE software includes list of fit parameters that can be modified to match experimental and modelling results. Then using the fit parameter model, parameters such as doped carrier plasma frequency and damping [45] were modified to find a fit between the computed and experimental values.

5.3 Comparison between Theoretical and Experimental Results

The theoretically simulated optical and device characterisations of CdTe solar cell stack has been compared with the experimentally obtained devices. In the experimental devices, CdS films were deposited on plain glass using chemical bath deposition technique and CdTe films using MOCVD technique. The thickness of CdS layer was varied from 60 to 250 nm. The thickness of CdS layers was measured using Dektak profilometer. Experimental values for transmittance for individual layers were obtained using a UV-Vis spectrophotometer. For transmittance measurements, plain float glass was used as a reference. Similarly for transmittance studies of CdTe layer, films were deposited using MOCVD method at Centre for Solar Energy Research (CSER), Glyndŵr University, with the help of Dr. Andy Clayton. The experimental details of preparation of CdTe films are given in chapter 4.

The transmittance (T) values for each of the component layers are shown. Transmittance in the figures is represented as a fraction (i.e. 1 means 100 % transmittance and 0 means 0% transmittance). Experimentally measured transmittance values were obtained using plain float glass as reference. Individual layers of CdS and CdTe were deposited on plain glass in a separate experiment so that the transmittance of individual layers could be studied. Transmittance of CdS layer on glass is depicted in figure 5.1. The transmittance of a 400 nm thick CdTe layer is shown in figure 5.2. The figures show both the simulated and experimentally measured spectra.

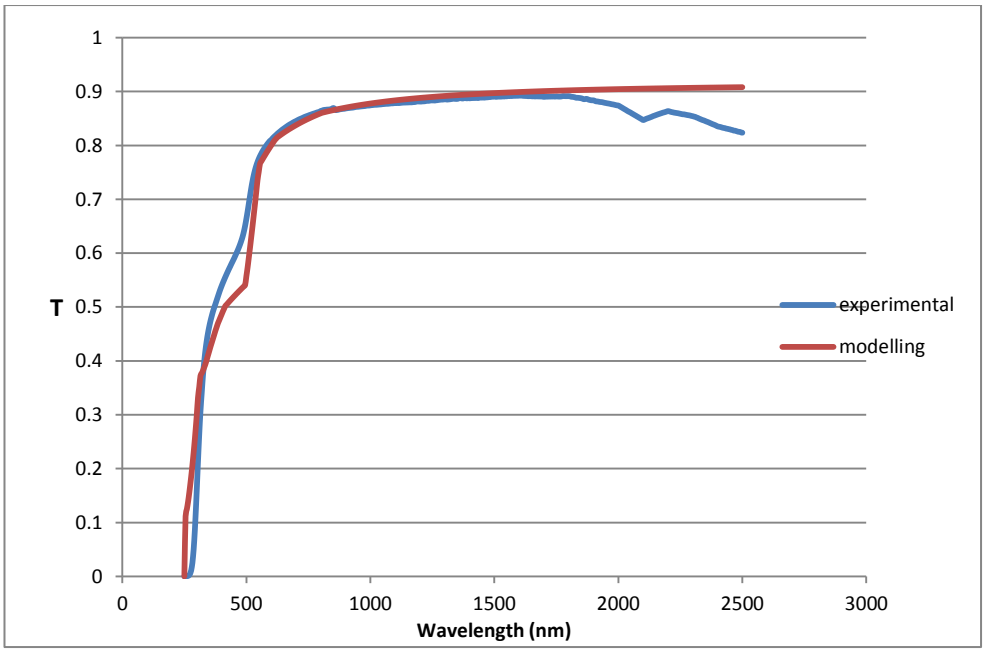

Figure 5.1 Transmittance spectra comparison for experimental and modelled CdS thin films

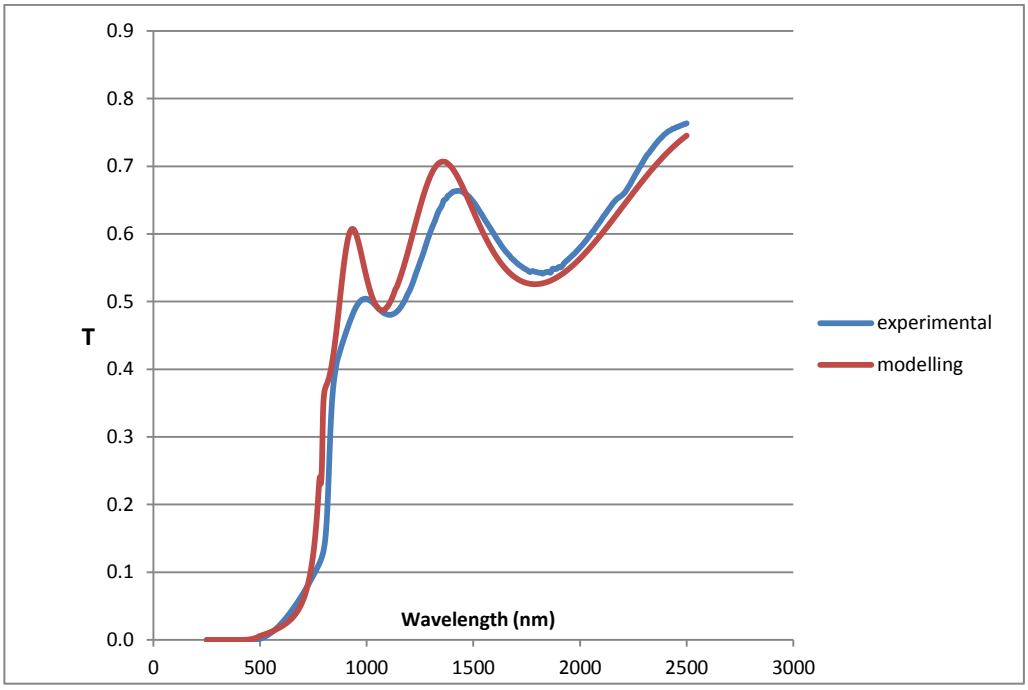

Figure 5.2 Transmittance spectra comparison for experimental and modelled CdTe thin films

Parameters carrier plasma frequency and damping were varied for the three layers. Once a satisfactory match was obtained for the individual layers, each component configuration was saved to be used in the next stage. In the second part of the experiment, the optical and electrical properties of ultrathin CdTe combined cell stacks were studied (Glass/TCO/CdS/CdTe stack) using simulation. The software allows us to stack up layers one on top of each other and simulate the optical spectra of the combination as a whole. The individual modelled layer parameters (obtained as above) were used to form a simple stack as shown. NSG-Pilkington TEC 7 glass coated with SnO_2:F (Fluorine doped tin oxide) was the base. CdS on top formed the window layer. CdTe formed the absorber layer on top of CdS to form the *p-n* junction. The stack is shown in the figure below.

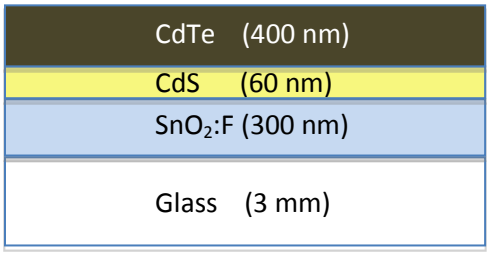

Figure 5.3 Schematic of CdTe solar cell stack used in the simulation

The objective was to vary thicknesses of window and absorber layers and study the transmittance of the stack in the visible spectrum of light. Also it was intended to determine the effect of progressive thinning down of layers on electrical response of the stack. Using an inbuilt module of the CODE software, the maximum probable photocurrent was calculated. CODE assumes a single active absorber layer that generates the majority of charge carriers by photon absorption. In this case it is the CdTe layer. The next assumption is that the active layer lies between two conducting layers. One of the conducting layers is a metal back contact. The other layer is a window layer of semiconductor CdS which allows most of the light to pass through. CODE uses the layer absorption to calculate the energy absorbed in the active layer. If the internal quantum efficiency of the device is known, the charge carriers available to electrical contacts can be calculated. Here CODE assumes generated carriers are immediately absorbed in to electrical contacts thus avoiding recombination losses at the contacts. The internal quantum efficiency is an indicator of the probability of an absorbed photon in the active layer to be converted into a charge carrier and further contribute to electrical current. The internal quantum efficiency data is taken as an average from the databases. The internal quantum efficiency is multiplied with the solar spectrum and integrated over the entire wavelength range from 250 to 2500 nm to generate photocurrent. The photocurrent values are generated in mA/cm^2. An illumination power of 1000 W/m^2 is used for the purpose. Here we have used photocurrent as an indicator of the electrical behaviour. The modelling results are presented as below.

5.3.1 Dependence on CdS thickness

CdS thickness was varied from 60 nm to 250 nm by keeping CdTe thickness of 400nm. Transmittance of the stack was studied for wavelength of light between 300 and 850 nm. The effects of varying thickness of CdS on the transmittance, as simulated by modelling are shown in the graph. Modelling data for transmittance of stack suggests that varying CdS thickness does not affect the transparency of the system considerably.

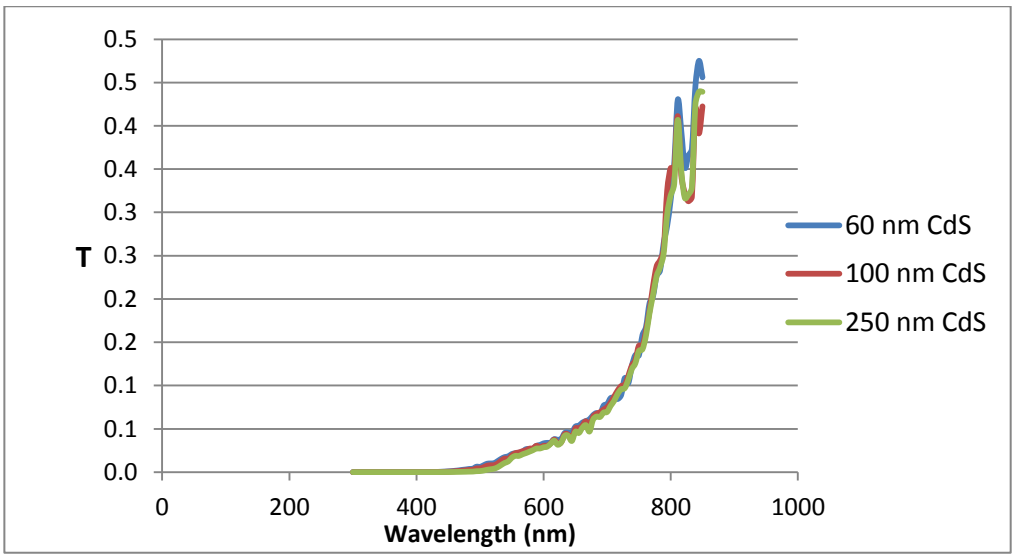

Figure 5.4 Transmittance spectra comparison for solar stack (TEC 7/CdS/CdTe) with different thicknesses of CdS thin films (simulated)

5.3.2 Dependence on CdTe thickness

Similarly thickness of the CdTe layer was varied from 1000 nm to 300 nm with constant thickness CdS of 60nm to study how the transmittance would improve on decreasing the absorber layer. The shapes of the waveforms for all widths of CdTe layers were similar but showed pronounced differences in the visible spectrum range as shown below. The graph clearly indicates that even at 500 nm thick CdTe layer transparency of the stack is very low.

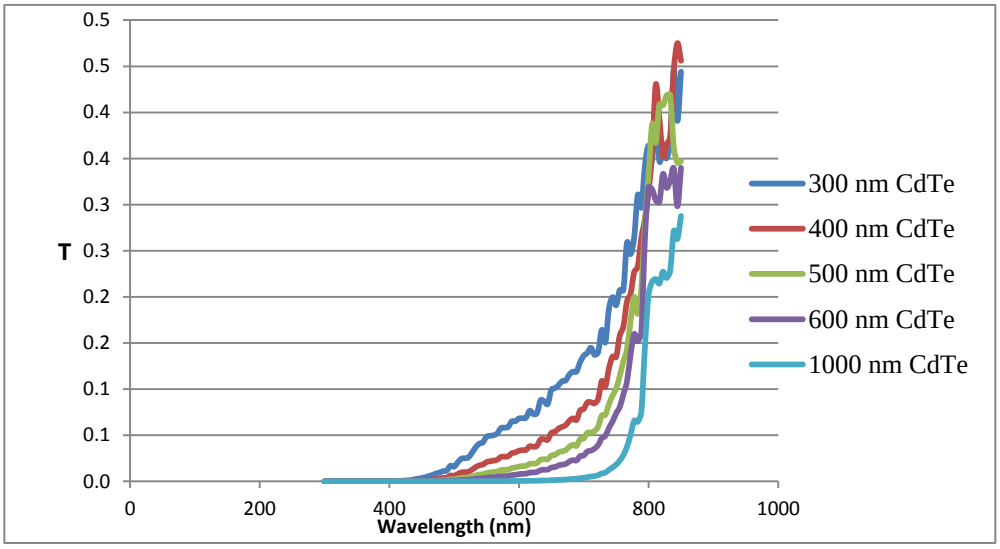

Figure 5.5 Transmittance spectra comparison for solar stack (TEC 7/CdS/CdTe) with different thicknesses of CdTe thin films (simulated).

5.3.3. Photocurrent Calculation

(a) Theoretical Modelling

An object of type 'layer absorption' in CODE allows estimation of light absorbed in an individual layer. In this case it needs to be the absorber layer. Then user defined quantum efficiency can be given as input to the program. Quantum efficiency (internal) referred to here, indicates the likelihood of an absorbed photon to generate a charge carrier and hence result in electrical current. The software calculates the energy absorbed in the absorber layer. The software assumes that Ohmic conductors photocurrent can be generated by multiplying the quantum efficiency with the solar spectrum over the desired wavelength range. AM 1.5 spectrum was used for the current study. The modelled results are tabulated in the table below.

CdTe Thickness (nm)	**CdS Thickness (nm)**	**Simulation Current Density (J_{sc}) (mA/cm^2)**	**Experimental Current Density (J_{sc}) (mA/cm^2)**
300	60	18.73	18.0
400	60	23.77	21.2
600	60	23.86	21.6
600	250	21.86	20.0
1000	250	23.40	9.5

Table 5.1 Simulated and experimental short circuit current (J_{sc}) values for different stack combinations

From figure 5.4 and table 5.1 we can see that, changing the thickness of the CdS layer from 60 to 250 nm has very little effect on the visibility of the stack, however, increasing the thickness causes a decrease in the photocurrent generated. Similarly studying figure 5.4 and table 5.1 together we can observe that decreasing CdTe thickness causes a decrease in the photocurrent while increasing the transparency. The difference in theoretical and experimental values in the case of 1000 nm CdTe device was large because the cell was damaged while forming the back contact.

(b) Experimental Results

Based on the modelling results, various layer combinations of CdS and CdTe using the standard procedures were prepared. The CdTe and CdS layers have been prepared by

MOCVD and CBD methods, respectively. The gold back contact for the different configuration of the CdTe cells was evaporated. The table 5.2 shows the experimental plans for the CdTe stack combinations with ultra-thin CdTe solar cells.

S.No	Substrate	CdS thickness (nm)	CdTe Thickness (nm)	Back contact
1	Glass/FTO TEC -7	250	1000	Gold
2	Glass/FTO TEC -7	250	600	Gold
3	Glass/FTO TEC -7	250	1000	
4	Glass/FTO TEC -7	250	600	
5	Glass/FTO TEC -7	60	600	Gold
6	Glass/FTO TEC -7	60	400	Gold
7	Glass/FTO TEC -7	60	300	Gold
8	Glass/FTO TEC -7	60	600	
9	Glass/FTO TEC -7	60	400	
10	Glass/FTO TEC -7	60	300	

Table 5.2 Experimental plan for ultrathin CdTe solar cells

As seen in the table above some of the samples were deposited with gold back contacts to complete the solar cell devices. J-V and EQE characteristics of these completed solar cell devices were studied. The remaining samples were left incomplete to measure the transmittance and compare the experimental results with the modelling results obtained above.

Table 5.1 lists the short circuit current density (J_{sc}) of the cells completed with gold back contact as well the modelled results. The difference in the modelled and experimental photocurrent values can be attributed to parasitic resistances in the actual devices. The measured resistances are shown in table 4.1. The transmittance results as predicted by the computer model and the experimental transmittance values are depicted in figure 5.6. The figure shows transmittance values for the entire stack TEC 7 Glass / CdS(60nm)/ CdTe(400 nm) taken using a UV-Vis spectrophotometer. The transmittance values range between 250 and 2500 nm of the solar radiation spectrum. The graph shows that the transmittance for a CdTe solar stack rises sharply after 500nm. It reaches a maximum value of 50 % and finally falls sharply at around 1000 nm. Also

depicted in the graph are the transmittance values generated from the computer model using the individual layers (previously generated) as building blocks. The graph shows close approximation between modelled and experimental values.

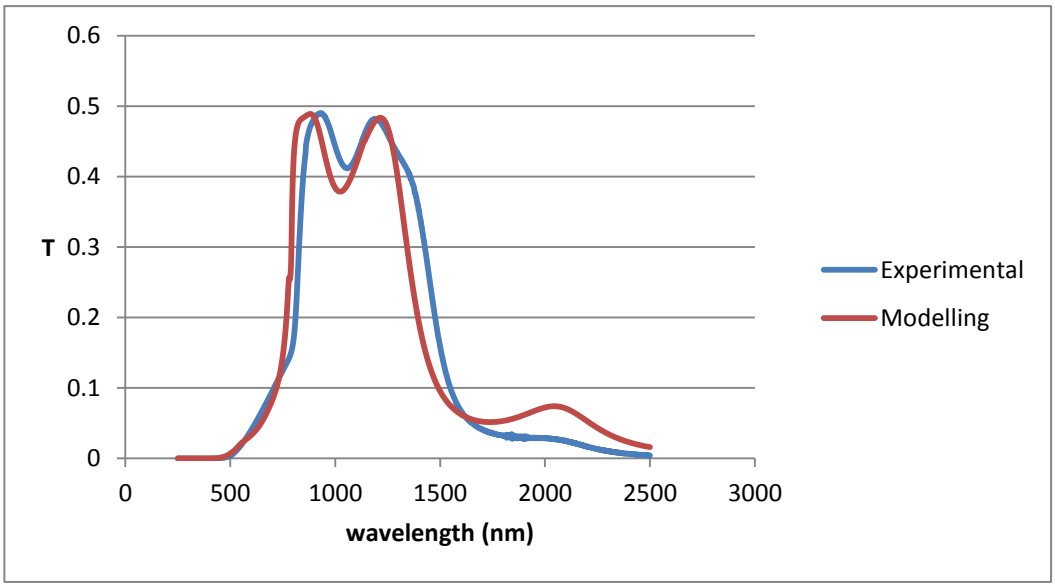

Figure 5.6 Transmittance spectra of solar stack CdTe (400)/ CdS (60)/ FTO

The transmittance remains less than approximately 20 % for the visible region. Higher transmission is observed for the red region while zero transmission was observed for the blue region. Low transmission in the visible region puts a limit on use of CdTe based cells in windows. However adding Zn to CdTe may improve transmission in the visible region. This possibility has been explored in the next chapter.

5.4 Conclusion

The experimental work was aimed at creating a computer model for CdTe based cells that could help predict optical and electrical properties and hence study CdTe cells better. Optical simulation of CdTe based solar cell stack was carried out using CODE software. CdTe thickness in the range of 300-1000 nm and CdS thickness in the range of 60-250 nm were studied. Modelled results were compared with experimental transmittance and short circuit current values. The experimental results conform closely with the modelling results.

Chapter 6: Optical Modelling of $Cd_{1-x}Zn_xTe$ for semi-transparent PV Windows Application.

6.1 Introduction

$Cd_{1-x}Zn_xTe$ or (CZT for convenience) is a ternary compound used as an absorber material for solar cells. In this compound, concentration of Zn, denoted by x can be modified by changing the deposition conditions and hence a control over the band gap of the resultant compound can be achieved. $Cd_{1-x}Zn_xTe$ alloy system has a band gap range, from 1.5 eV (x = 0) to 2.24 eV (x = 1) [28]. $Cd_{1-x}Zn_xTe$ is structurally similar to CdTe crystallizing in the zinc blende structure. The preparation procedures are easy and scalable and similar to fabrication procedures used for CdTe. For solar cell applications, deposition methods for CZT include sputtering, molecular beam epitaxy, vapour transport [49]. CZT is also known to form good interface with common window material CdS. This chapter summarises the optical modelling based on alternative absorber materials for CdTe solar cells.

6.2 Modelling

With the possibility of having a wider band gap for CZT absorber layer, a higher transmission can be achieved, especially in the visible range, a limiting factor in the case of CdTe cells. In this study, we try and simulate the optical properties of a solar cell stack. Here absorber layer of CdTe has been replaced by the ternary compound group $Cd_{1-x}Zn_xTe$. CZT can have increased transparency in the visible region compared with a similar thickness CdTe layer. The cost of increased transparency is reduced conversion efficiency. However, since the intended use of the CZT solar stacks being developed is in window glazing, higher transmission is very important. Thus the effort is to evaluate whether CZT can be an alternative to CdTe absorber layers.

The stack to be modelled is shown below in figure 6.1 with stacked layers of the device Glass (3 mm)/ FTO(300 nm)/ CdS(60 nm)/ $Cd_{1-x}Zn_xTe$ (400 nm). Except $Cd_{1-x}Zn_xTe$ layers, all other layer thicknesses have been kept same for a comparison with previously studied CdTe.

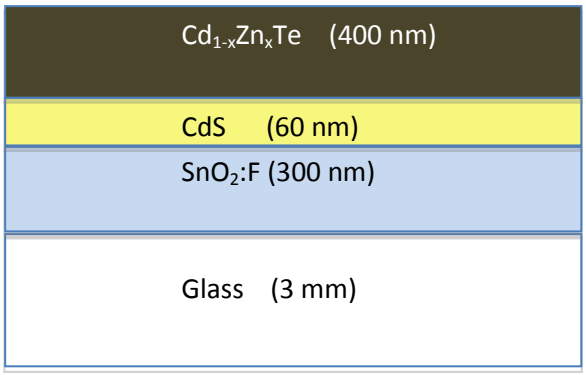

Figure 6.1 CZT based solar stack with approximate thickness of each layer shown.

For this purpose, five concentration combinations of the $Cd_{1-x}Zn_xTe$ compound group were selected.

a) $Cd_{0.9}Zn_{0.1}Te$

b) $Cd_{0.7}Zn_{0.3}te$

c) $Cd_{0.5}Zn_{0.5}Te$

d) $Cd_{0.3}Zn_{0.7}Te$

e) $Cd_{0.1}Zn_{0.9}Te$

For the selected concentration combinations, n and k values were obtained from the dielectric function databases. The n, k value set can be fed into CODE software. The CZT layer was put at the top of the basic stack, as used in previous study in this thesis. The components of the basic stack – namely CdS layer, SnO_2:F layer and glass layer were kept the same as used for the previous study. The figure 6.2 below depicts the transmittance (simulated) of a 4 layer solar cell stack comprising CZT(400nm)/ CdS(60nm)/ SnO_2:F(350 nm)/Glass (3 mm). The absorber layer in the stack is CZT which differs from one combination to another in Zn concentration. Figure 6.2 shows transmittance over the wavelength region 250nm to 2500 nm. Transmittance, reflectance and absorption are shown as fractions (i.e. 1 means 100 % transmittance and 0 means 0 % transmittance). As can be seen, the transmittance behaviour of the different combinations is identical over the IR and the UV regions. However, the transparency of the stack combinations varies significantly over the visible part of the solar spectrum. As the Zn concentration increases, the left transparency edge shifts more towards lower wavelengths thus allowing more light to pass through. The region between 400 – 600 nm sees the most prominent shifts in this regard. As the rest of the transmittance spectrum remains the same, it is reasonable to suggest that if a selection for the absorber

material were to be made with the main criteria of higher optical transparency, a CZT layer higher in Zn would be the material of choice.

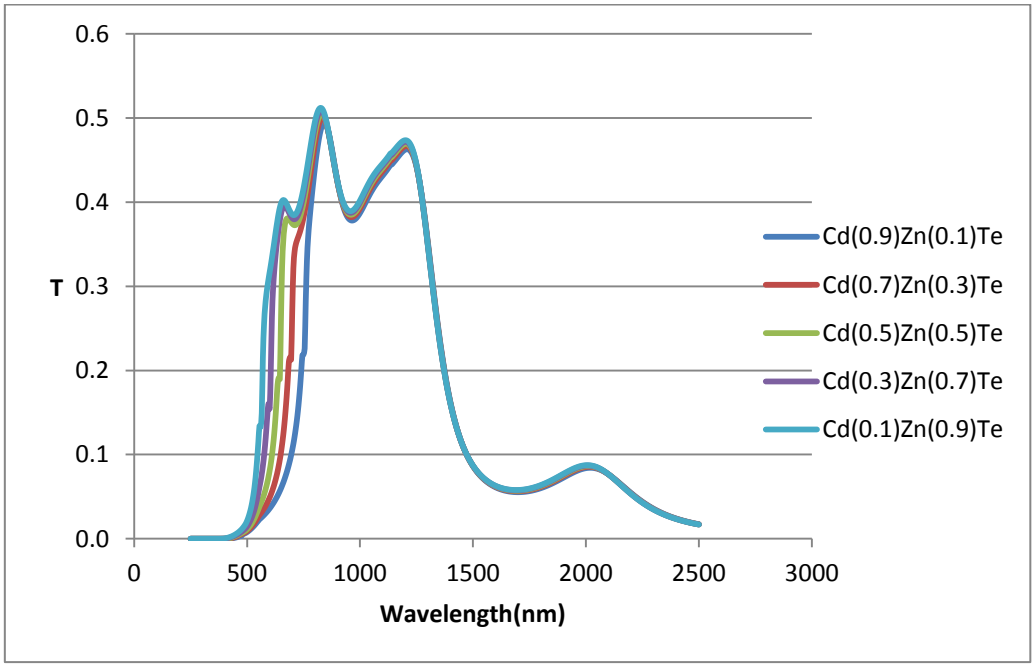

Figure 6.2 Transmittance of the solar stack with CZT (400nm) between 250 – 2500 nm (normalised).

Another parameter under study is the layer absorption in CZT absorber layers. The percentage of energy absorption in CZT layers decreases with increasing Zn concentration, depicting layer absorption between 250 nm and 2500 nm is consistent with the transmission data. This reflects that maximum change over the degree of absorption occurs over the visible range.

Figure 6.3 depicts the simulated reflectance data of CZT based stacks. The reflectance behaviour of the wavelength spectrum ranging from 250 nm to 2500 nm shows little or no difference amongst $Cd_{1-x}Zn_xTe$ (x= 0.1 to 0.9). Further, the variations obtained look spurious. Unfortunately, no conclusive interpretation of this result can be made as this does not fit with the transmission and absorption results. Although it was an ambitious attempt to fit the values of the five CZT variants from the scientific database but it appears the CODE software may not be working well. Thus, an experimental validation of above results will be much needed to come to a firm conclusion and will help understand the limitation of the CODE software.

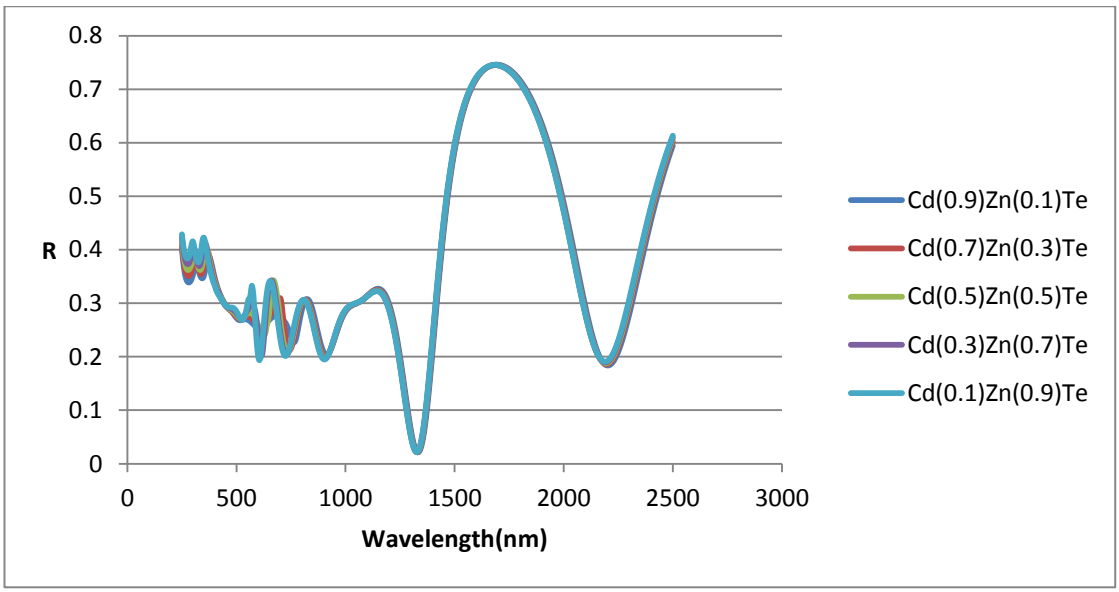

Figure 6.3 Reflectance of CZT (400nm) based solar stack between wavelengths 250 – 2500 nm (normalised).

The CODE software allows an estimation of the maximum short circuit current from a solar cell stack. As done is previous chapter, the CODE assumes a single active absorber layer that generates the majority of charge carriers by photon absorption. In this case it is the CZT layer.

The J_{sc} values for the different CZT solar cell combinations with varying absorber layer thickness are shown in the table 6.1.

Absorber material	**Current Density (J_{sc}) (mA/cm^2)**		
	200 (nm)	**300 (nm)**	**400 (nm)**
$Cd_{0.9}Zn_{0.1}Te$	12.42	13.98	15.86
$Cd_{0.7}Zn_{0.3}te$	11.48	12.98	14.74
$Cd_{0.5}Zn_{0.5}Te$	10.67	12.11	13.97
$Cd_{0.3}Zn_{0.7}Te$	9.98	11.39	13.23
$Cd_{0.1}Zn_{0.9}Te$	9.35	10.7	11.89

Table 6.1 Theoretical photocurrent values for various thicknesses of absorber layer using CODE software.

The J_{sc} values show a decreasing trend with increasing Zn concentration. Also the absorber layer thickness decreases the photocurrent generated decreases. This trend is also manifested by the optical transmittance behaviour of the solar cell stacks.

6.3 Conclusions

Solar stacks based on absorber material as $Cd_{1-x}Zn_xTe$ with varying concentrations of Zn were modelled using CODE. The simulated transmittance results indicate an increasing transparency in the visible region with higher Zn content. The transmittance in visible range was close to 40 %. Energy absorption in the absorber layer expectedly decreases with increasing Zn and decreasing Cd content. This trend is reflected in the lowering of photocurrent values. A lowest case J_{sc} of 9.35 mA/cm^2 was obtained for a stack containing 200 nm thick $Cd_{1-x}Zn_xTe$ absorber layers. If experimental results conform to the modelling studies conducted here, CZT can prove to be useful absorber material in ultrathin solar cell applications.

Chapter 7: Conclusions and Scope for Future Work

7.1 Conclusions

The project work was divided into four parts.

In the first part, cadmium telluride films were prepared by electrodeposition process. The electrodeposited films were uniform in nature with thickness around 1 micron. SEM studies were conducted to study the surface morphology. Although the required phases of CdTe were obtained as was also confirmed by the characterisation studies but it was found to contain substantial oxygen and sulphur impurities, which essentially were coming from electrolytic bath with additives such as from sulphuric acid to maintain the pH of the solution and formation of CdO phases. This learning will be exploited in making better quality films. One approach will be to use non-aqueous medium with high purity precursors, which can avoid water (Hydrogen and Oxygen in the over-potential region) and acid related ions.

In the second part ultra-thin CdTe/CdS solar cells were prepared using MOCVD process for CdTe layer and chemical bath deposition for CdS. Efficiencies of 6.8 % for 600 nm CdTe and 4.9 % for 400 nm CdTe were observed. Even 300 nm thick CdTe cells showed efficiency greater than 4 %, which was very encouraging result. Cells suffered from low shunt and high series resistance, which was obvious as this may be coming from the pinholes and undulations almost 150- 200 nm from the FTO layer on glass supplied by NSG-Pilkington. The cell performance can be enhanced by using planarised layers on FTO, which will be planned in the future.

The third part of the experimental work was aimed at creating a computer model for CdTe based cells that could help predict optical and electrical properties and hence study ultra-thin CdTe cells better. Optical simulation of CdTe based solar cell stack was carried out using CODE software. CdTe thickness in the range of 300- 1000 nm and CdS thickness in the range of 60-250 nm were studied. Modelled results were compared with experimental transmittance and short circuit current values. The experimental results conform closely with the modelling results.

Finally, solar stacks based on absorber material as $Cd_{1-x}Zn_xTe$ with varying concentrations of Zn were modelled using CODE. This was an ambitious attempt to

generate new data sets from the CODE software based on the data on bandgap, n and k values of various compositions of the CZT layers. However, this may have had limitations in the results to follow as this was done for the first time using CODE software. The simulated transmittance results indicate an increasing transparency in the visible region with higher Zn content, which looks obvious and encouraging. The transmittance in visible range was close to 40%. Energy absorption in the absorber layer expectedly decreases with increasing Zn and decreasing Cd content. This trend is reflected in the lowering of photocurrent values. Unfortunately, the reflectance data was not matching with the transmission data where the trend looked bit spurious and inconclusive. A lowest case J_{sc} of 9.35 mA/cm^2 was obtained for a stack containing 200 nm thick $Cd_{0.1}Zn_{0.9}Te$ absorber layer. It remains to be checked with the experimental studies for five set of CZT compositions. The experimental validation of the modelling studies conducted here can prove to be useful in recommending CZT absorber material in ultra-thin solar cell applications.

7.2 Future Work Recommendations

1. Modelling of the solar cell stack has enabled us to establish theoretically the optical properties of the individual layers. Further modelling work needs to be carried out to optimise the absorption and the transparency of the solar stack particularly in the optical range. Haze measurements need to be included in the optical study of the stack.

2. Optical study done until now has shown that the designed solar stack had high reflectance in the infrared region, which needs a confirmation through experimental data sets and perhaps may need modification of the CODE software itself.

3. It needs to be attempted to include certain optical layers in the stack which may allow better absorption in the infrared region as well. Moreover, it may be attempted to include layers in the design which may allow colour of the stack to be changed to suit architectural needs.

4. Further work should involve working on low cost non vacuum methods to fabricate CdTe based solar cells. Efforts need be directed towards electrodeposition of CdTe to carry on the work done previously and precursors such as $CdSO_4$ may be replaced by $CdCl_2$ to try and reduce one crucial step (of $CdCl_2$ treatment) in CdTe solar cell processing. MOCVD based CdTe cells showed good results and further studies using

the process can allow CdTe or $Cd_{1-x}Zn_xTe$ based solar cells with higher transmittance and even lower thickness of the absorber layer.

References:

[1] World Wildlife Fund, (2010) http://wwf.panda.org/__what_we_do/footprint/climate_carbon_energy/energy_solutions/renewable_energy/sustainable_energy_report

[2] Hari M Upadhyaya, S.Senthilarasu, Min Hung Hsu, D. Kishore Kumar, Solar Energy Materials &Solar Cells119(2013)291–295

[3] Siwei Li, Panagiota Solar Energy 102 (2014) 297–307

[4] U.S. Department of Energy, Energy Efficiency and Renewable Energy,. http://www1.eere.energy.gov/solar/pdfs/solar_timeline.pdf

[5] Soohyun Kim, Jin-Won Chung, Hyun Lee, Jinhee Park, Younho Heo, Heon-Min Lee Solar Energy Materials & Solar Cells119 (2013) 26–35

[6] Martin Günthner, MarkusPscherer, Christian Kaufmann, Günter Motz Solar Energy Materials& Solar Cells 123 (2014) 97–103

[7] Armin G. Aberle, Thin Solid Films 517 (2009) 4706–4710

[8] Frank L. Riley Journal of the American Ceramics Society 83 (2000) 245-265

[9] Martin A. Green, Keith Emery, Yoshihiro Hishikawa, Wilhelm Warta and Ewan D. Dunlop, Progress in Photovoltaics : Research and Applications , 20 (2012) 606-614

[10] Danny H.W. Li , Tony N.T. Lam, K.L. Cheung Energy Conversion and Management, 50 (8) , (2009) 1981-1990

[11] University of Minnesota, http://www.commercialwindows.org/vt.php

[12] K Zanio Semiconductors and Semimetals, Vol. 13 (Cadmium Telluride) (1978)

[13] J.L. Loferski, J. Appl. Phys. 27 (1956) 777.

[14] Rodot, Second International Symposium on CdTe, Strasbourg, 1976; Rev. Phys. Appl. 12 (2) (1977) 411.

[15] D.R. YoderShort, U. Debska, J.K. Furdyna J. Appl. Phys. 58 (1985) 4056.

[16] M.G. Peters, A.L. Fahrenbruch, R.H. Bube, J. Vac. Sci. Technol. A6 (1988) 3098.

[17] S. Sen, H. Konkel, S.J. Tight, L.G. Bland, S.R. Sharma, R.E. Taylor, J. Crystal Growth 86 (1988)

[18] S. Lalitha, R. Sathyamoorthy, S. Senthilarasu, A. Subbarayan, K. Natarajan Solar Energy Materials & Solar Cells 82 (2004) 187–199

[19] H. R. Moutinho, F. S. Hasoon, F. Abulfotuh and L. L. Kazmerski J. Vac. Sci. Technol. A 13 (1995) 2877

[20] T Aramoto, S Kumazawa, H Higuchi, T Arita, S Shibutani, T Nishio, J Nakajima, M Tsuji, Akira Hanafusa, T Hibino, K Omura, H Ohyama and Mikio Murozono Jpn. J. Appl. Phys. 36 (1997) 6304

[21] T Okamoto, Y Harada, A Yamada, M Konagai Solar Energy Materials & Solar Cells 67 (2001) 187-194

[22] H. R. Moutinho, R. G. Dhere, M. M. Al-Jassim, D. H. Levi and L. L. Kazmerski J. Vac. Sci. Technol. A 17, (1999)1793

[23] T. L. Chu, S. S. Chu, C. Ferekides, C. Q. Wu, J. Britt and C. Wang J. Appl. Phys. 70 (1991)7608

[24] H. R. Moutinho, M. M. Al-Jassim, D. H. Levi, P. C. Dippo and L. L. Kazmerski J. Vac. Sci. Technol. A 16 (1998)1251

[25] G Gordillo,, JM Florez, LC Hernandez, Solar Energy Materials and Solar Cells 37 (1995) 273-281

[26] N Romeo, A Bosio, V Canevari, A Podesta Solar Energy 77 (2004) 795–801

[27] J Luschitz, K Lakus-Wollny, A Klein, W Jaegermann Thin Solid Films 515 (2007) 5814–5818

[28] B. Basol , V. Kapur , R. Kullberg , 20th IEEE Photovoltaic Specialist Conference, 1500–1504, (1988).

[29] T. L. Chu, S. S. Chu, C. Ferekides, and J. Britt , J. Appl. Phys., 71 (1992) 5635

[30] A. Luque, S. Hegedus(eds.), John wiley and Sons, , (2007) 602

[31] C. S. Ferekides, D. Marinskiy, V. Viswanathan, B. Tetali, V. Palekis, P. Selvaraj, D. L Morel Thin Solid Films, 361 (2000)520-525

[32] B.E. McCandless, R. W. Birkmire, W. A. Buchanan, Photovoltaics Specialists Conference , (2002) 547 550

[33] B. L. Williams, R. E. Trehame and K. Durose Proceedings of PVSAT-6 March (2010)

[34] V. M. Nikale, S. S. Shinde, C. H. Bhosale and K.Y. Rajpure Journal of Semiconductors, 32 (2011) 30

[35] B.M Baosl Journal of Applied Physics,55 (1984)601-603

[36] A Nouhi, R J Stirn, P V Meyers, C H Liu , Journal of Vacuum Science & Technology A: Vacuum, Surfaces, and Films, 7 (1989) 833-836

[37] N. Nakayama, H. Matsumoto, A. Nakano, S. Ikegami, H. Uda and T. Yamashita, Japanese Journal of Applied Physics, 19 (1980)703-712

[38] J. Poortmans and V. Arkhipov John Wiley & Sons,(2006) 286-294

[39] X. Mathew, G. W. Thompson, V.P. Singh, J.C. McClure, S. Velumani, N.R. Mathews, P.J. Sebastian,. Solar Energy Materials & Solar Cells 76 (2003)293–303

[40] A. Romeo, , Thesis , Swiss federal Institute of technology, (2002)

[41] C S Ferekides, U Balasubramaniam, R. Mamazza, V. Viswanathan, H. Zhao, D.L. Morel, Solar energy, 77 (2004) 823-830.

[42] D.Bonnet, P.Meyers , Journal of Materials Research, 13 (1998) 2740-2753

[43] I. M. Dharmadasa and J. Haigh Jassim Journal of Electrochemical Society,153 (2006)G47-G52

[44] M. P. R. Panicker, M. Knaster, and F. A. Kroger Journal of Electrochemical Society, 125 (1978)566-572.

[45] Heriot watt /Glyndwr Collaboration study report (2012)

[46] M Fox Oxford University Press (2007)

[47] W Theiss, Technical Manual for SCOUT/CODE software (2008)

[48] A. Rohatgi , S.A. Ringel , R.Sudharsanan Solar Cells, 27 (1998)219-230

[49] A.Rohatgi, R.Sudharsanan, S.A.Ringel, , Solar Cells, 30 (1991)109-122

[50] S.J.C. Irvine, D.A. Lamb, V. Barrioz, A.J. Clayton, W.S.M. Brooks, S. Rugen-Hankey, G. Kartopu, , Thin Solid Films, 520 (2011) 1167-1174